

Inclusive Production Cross Sections at N^3LO

JULIEN BAGLIO,^a CLAUDE DUHR,^b BERNHARD MISTLBERGER,^c AND
ROBERT SZAFRON^d

^a*Theoretical Physics Department, CERN, Esplanade des Particules 1, 1217 Meyrin,
Switzerland*

^b*Bethe Center for Theoretical Physics, Universität Bonn, D-53115, Germany*

^c*SLAC National Accelerator Laboratory, Stanford University, Stanford, CA 94039,
U.S.A.*

^d*Department of Physics, Brookhaven National Laboratory, Upton, N.Y., 11973, U.S.A.*

Abstract

We present for the first time the inclusive cross section for associated Higgs boson production with a massive gauge boson at next-to-next-to-next-to-leading order in QCD. Furthermore, we introduce `n3lox`, a public, numerical program for the evaluation of inclusive cross sections at the third order in the strong coupling constant. Our tool allows to derive predictions for charged- and neutral-current Drell-Yan production, gluon- and bottom-quark-fusion Higgs boson production and Higgs boson associated production with a heavy gauge boson. We discuss perturbative and parton distribution function (PDF) uncertainties of the aforementioned processes. We perform a comparison of global PDF sets for a variety of process including associated Higgs boson production and observe 1σ deviations among predictions for several processes.

Contents

1	Introduction	3
2	Inclusive color singlet production in QCD	5
3	Phenomenological results for Higgs and Drell-Yan production	7
3.1	Scale dependence and scale uncertainties	8
3.2	PDF study for Drell-Yan and Higgs processes	9
4	Inclusive associated VH production at N^3LO	25
4.1	Inclusive cross sections and scale uncertainties	25
4.2	Study of the PDF sets and associated PDF, PDF+ α_S and PDF-TH un- certainties	27
5	Comparison of N^3LO predictions	33
6	Summary and conclusions	35
A	n3loxS	36
A.1	Installation	37
A.2	Usage	38
B	Parameters	40
C	Inclusive cross sections for VH processes at various additional center- of-mass energies	42
D	Binned cross sections for Drell-Yan processes	45

1 Introduction

Experimental high-energy physics is at the dawn of a new precision era. Run 3 of the Large Hadron Collider (LHC) at CERN and its subsequent upgrade to the High-Luminosity LHC will bring a plethora of further data. These efforts on the experimental side must be met with a solid push towards more accurate and precise theoretical predictions. So far, the Standard Model (SM) has been highly successful in describing data across many scales and processes. This success has been possible thanks (among other things) to reasonable control over QCD effects, which dominate at hadron colliders. Next-to-leading order (NLO) corrections are now routinely available for the SM backgrounds and predicted signals of new physics. The past few years have seen a surge of next-to-next-to-leading order (NNLO) computations, and nowadays, many differential observables are known at NNLO accuracy. Still, very little is known about the third-order corrections (N³LO), with the first prediction for single Higgs production at the LHC becoming available in 2015 [1], and the very first differential observable for the same process having been computed only very recently [2]. Since this very first differential calculation more results focusing on Drell-Yan processes have been released in the past few months, see refs. [3–7]. Inclusive processes for the production of a colorless final state are typically the simplest to compute, and thus they are the first step in pushing the frontier of QCD perturbative computations. Recent years have brought significant progress in evaluating the N³LO corrections to inclusive color singlet production cross sections. This endeavor started with the evaluation of the gluon fusion Higgs production cross section [1, 8–14]. Shortly after the Vector Boson Fusion (VBF) cross section for Higgs boson production was obtained at N³LO with very different methods [15]. Today W -boson and photon mediated Drell-Yan cross sections are also known at the third order in the strong coupling constant α_S [16, 17], as well as the computation of the N³LO QCD predictions for Higgs production in bottom-quark fusion in the five-flavor scheme [18] (including the matching to the four-flavor scheme [19]) and the calculation of the gluon fusion and VBF double Higgs boson production cross sections [20, 21]. Recently, the computation of the Drell-Yan cross section was completed at N³LO with the calculation of the Z boson production cross section [22]. All these computations share many similarities. One of the main results of this paper is to introduce the new public computer code `n3lox`, which allows us to evaluate the N³LO inclusive cross sections for a variety of hadron collider processes.¹ We then use our code and present a comprehensive phenomenological study of these processes, at pp colliders, and, for the first time, also at $p\bar{p}$ colliders.

Inclusive cross sections play a variety of roles in high-energy phenomenology, ranging from precision tests of the SM to serving as standard candles for luminosity measurements. Furthermore, they provide a unique testing ground to study the progression of

¹There already exist dedicated codes for evaluation of the N³LO Higgs production cross section, such as `iHixs 2` [23], `ggHiggs` [24] and `SusHi` [25]. Note also that for Higgs production in vector-boson fusion, which is not included in our tool, there also exists a public tool for the evaluation of the cross section called `proVBFH` [15]

predictions obtained with increasing order in the perturbative expansion of scattering cross sections. Deriving reliable estimates of the uncertainty due to the truncation of the perturbative expansion plays a role of increasing importance as experimental results become more precise. Today’s standard paradigm is to estimate the size of the corrections neglected due to the truncation of the perturbative expansion by varying the unphysical renormalization and factorization scales. Only terms beyond the highest computed perturbative order are sensitive to the value of these scales, and the magnitude of the variation of the prediction is interpreted as an uncertainty. As the perturbative order is increased, the size of scale variations is expected to diminish, leading to quantitatively better results. Studying the progression of the perturbative series then serves as a test of this method to estimate uncertainties. Note that alternative approaches to estimating missing higher-order uncertainties were discussed for example in refs. [26–28].

In refs. [16, 17, 22], a significant cancellation of contributions to the total cross section from different partonic initial-state channels was observed. Individual partonic channels are weighted (or convoluted) with their respective parton distribution functions (PDFs). A small change in the PDF of one parton with respect to others might consequently result in a significant change of the predicted cross section. This observation raises a series of questions: Are these cancellations relevant only for proton-proton collisions, or do they also appear in proton-antiproton initiated processes, such as those studied at the former Fermilab Tevatron collider? Do missing N³LO PDFs play an essential role, and how much do our N³LO predictions depend on the choice of the PDF set? We are going to discuss these questions on examples of different processes using the N³LO perturbative results. This paper provides a comprehensive study of the impact of the choice of the PDF and the associated 68% confidence level (CL) PDF uncertainties on a variety of processes at N³LO. We compare the latest releases of the major PDF sets for hadron colliders to a nominal PDF set released in 2015 as a statistical combination of three global sets.

We will also present for the first time results for associated $W^\pm H$ and ZH production at N³LO in QCD. These so-called Higgsstrahlung processes are characterized by large masses of the final-state particles, which cannot be neglected, as it is customarily done for leptons. We provide both the total cross section and results binned according to the invariant mass of the pair of a massive weak boson with a Higgs boson. We discuss the theoretical uncertainties due to scale variation and PDFs, providing also the correlated PDF+ α_S uncertainty as well as the uncertainty related to the missing N³LO PDF set.

This paper is organized as follows. In section 2 we introduce the main calculational framework and the needed formulae for inclusive color singlet production at hadron colliders. The phenomenological results for Higgs and Drell-Yan production are given in section 3. We present the analysis of the variation of the PDF sets and the corresponding PDF uncertainties at the LHC at 13 TeV, including also validation plots for scale variation. The new predictions at N³LO in QCD for inclusive Higgsstrahlung production at hadron colliders, $pp/p\bar{p} \rightarrow VH$ with $V = W^\pm, Z$, are given in section 4. We compare N³LO predictions for different processes in section 5. A conclusion is provided in section 6. We also include three appendices. Appendix A explains in detail how

to install and use our public code `n3loxs`. Appendix B provides the reader and user of `n3loxs` with the physical parameters used in our predictions. Appendices C and D collect additional results for associated Higgs production at proton-proton colliders for various center-of-mass energies as well as binned invariant-mass distributions for Drell-Yan processes.

2 Inclusive color singlet production in QCD

The focus of this paper are QCD corrections to hadron collider processes for the s -channel production of a colorless final-state B of invariant mass Q :

$$N_1(P_1) + N_2(P_2) \rightarrow B(Q) + X, \quad (1)$$

where $N_i(P_i)$ is either a proton or antiproton with momentum P_i , and X represents arbitrary QCD final-state radiation. In the following we will be inclusive in the QCD radiation X and we are interested in the production cross section differential in Q^2 .

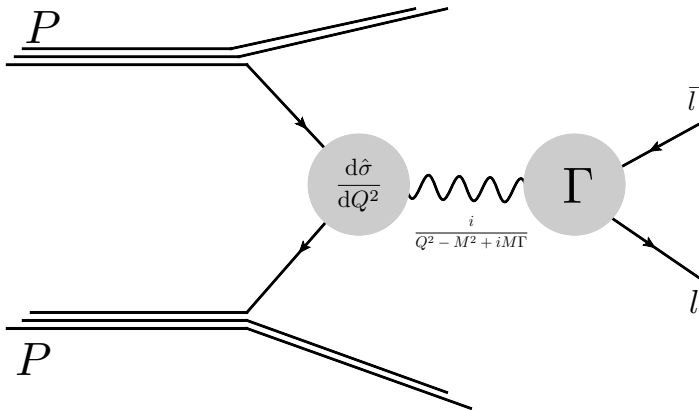


Figure 1: Schematic depiction of the Drell-Yan process and its factorization into the production probability of a virtual gauge boson and subsequent decay to final-state leptons.

If the widths of all intermediate s -channel states are small, we can think of this process in a factorized form involving three distinct steps. First, energetic partons collide and produce one (or more) off-shell colorless s -channel resonances. This part is described by short-distance partonic cross sections convoluted with the parton distribution functions (PDFs). These resonances then propagate over a short distance. Since we assume that the widths are much smaller than the mass, the propagation can be described by a relativistic Breit-Wigner formula. Finally, the intermediate particles decay into the color-singlet final-state particles with a probability determined by the partial decay width. The prototypical example of such a process is the Drell-Yan production process [29], which

describes the production of a lepton/antilepton pair in proton-proton collisions via an off-shell photon or Z -boson (see fig. 1). In the case where the final state B consists of a pair $f_1 f_2$ of particles with mass m_{f_i} , the cross section differential in the invariant mass Q^2 can be cast in the form:

$$\begin{aligned} \Sigma_{N_1 N_2 \rightarrow f_1 f_2 + X}(Q^2) &\equiv Q^2 \frac{d\sigma_{N_1 N_2 \rightarrow f_1 f_2 + X}}{dQ^2} = \\ &= \sum_{V, V'} Q^2 \frac{d\sigma_{N_1 N_2 \rightarrow V/V' + X}}{dQ^2} \times \text{BW}(Q^2, m_V, m'_V) \times \Gamma_{V/V' \rightarrow f_1 f_2}(Q^2, m_{f_1}^2, m_{f_2}^2). \end{aligned} \quad (2)$$

The propagation of the virtual s -channel states V and V' is described by the relativistic Breit-Wigner distribution,

$$\text{BW}(Q^2, m_V, m'_V) = \frac{Q^3}{\pi} \Re \left[\frac{1}{(Q^2 - m_V^2) + im_V \Gamma_V} \frac{1}{(Q^2 - m_{V'}^2) - im_{V'} \Gamma_{V'}} \right], \quad (3)$$

where \Re denotes the real part and $m_{V^{(l)}}$ and $\Gamma_{V^{(l)}}$ the on-shell mass and total decay width of the state $V^{(l)}$ respectively. The decay is described by the interference of the decay matrix elements integrated over the phase-space of the final-state particles $f_1 f_2$:

$$\Gamma_{V/V' \rightarrow f_1 f_2}(Q, m_{f_1}, m_{f_2}) = \frac{1}{2Q N_{\text{spin}}} \int d\Phi_2 \mathcal{M}_{V \rightarrow f_1 f_2} \cdot \mathcal{M}_{V' \rightarrow f_1 f_2}^*, \quad (4)$$

where N_{spin} denotes the number of spin states of V , i.e., $N_{\text{spin}} = 3$ if $V^{(l)}$ is a massive (axial-)vector and $N_{\text{spin}} = 1$ if it is a scalar, and $d\Phi_n$ denotes the n -body phase-space measure in d dimensions:

$$d\Phi_n = (2\pi)^d \delta^d \left(Q - \sum_{f=1}^n p_f \right) \prod_{f=1}^n \frac{d^d p_f}{(2\pi)^{d-1}} \delta_+(p_f^2 - m_f^2). \quad (5)$$

The quantity $\mathcal{M}_{V \rightarrow f_1 f_2} \cdot \mathcal{M}_{V' \rightarrow f_1 f_2}^*$ denotes the interference of the matrix elements, summed over all color and spin quantum numbers of all external particles. The above definition is chosen such that, if the formula is evaluated on-shell, $Q = m_V$ and $V = V'$, then it corresponds to the partial width $\Gamma_{V \rightarrow f_1 f_2}$ of the state V in its rest-frame,

$$\Gamma_{V \rightarrow f_1 f_2} = \Gamma_{V \rightarrow f_1 f_2}(m_V, m_{f_1}, m_{f_2}). \quad (6)$$

The remaining factor in eq. (2) is the total inclusive two-to-one cross section for the production of a color-singlet (axial-) vector or (pseudo-) scalar state V with virtuality Q^2 (or the interference in the case $V \neq V'$). It is obtained by convolution of the partonic coefficient functions with the PDFs:

$$Q^2 \frac{d\sigma_{N_1 N_2 \rightarrow V/V' + X}}{dQ^2} = \tau \sum_{i,j} \int_0^1 dx_1 dx_2 dz \delta(\tau - zx_1 x_2) f_{i/N_1}(x_1) f_{j/N_2}(x_2) \eta_{ij \rightarrow V/V' + X}(z), \quad (7)$$

with

$$\tau = \frac{Q^2}{s} \quad \text{and} \quad s = (P_1 + P_2)^2, \quad (8)$$

and $f_{i/N_k}(x_k)$ denotes the PDF to find a parton species i with momentum fraction x_k inside the hadron N_k . We see that the computation of inclusive cross sections for s -channel mediated color-singlet production can be reduced to the computation of the coefficient functions for inclusive two-to-one processes. The coefficient functions for (axial-)vector production from quark annihilation and (pseudo-)scalar production from quark annihilation as well as gluon fusion were computed up to NNLO in the strong coupling constant more than two decades ago [30–56]. Very recently also N³LO corrections to inclusive color-singlet production of scalar, vector and axial-vector states have become available. In the next sections, we discuss phenomenological predictions for the following processes.

- Drell-Yan production: $N_1 N_2 \rightarrow \gamma^*/Z \rightarrow \ell^+ \ell^-$ [16, 22],
- Charged-Current Drell-Yan production: $N_1 N_2 \rightarrow W^\pm \rightarrow \ell^\pm \bar{\nu}_\ell$ [17],
- On-shell Higgs production $N_1 N_2 \rightarrow H$ from both gluon and bottom-quark fusion [1, 18],
- Higgsstrahlung $N_1 N_2 \rightarrow HV$, with $V \in \{Z, W^\pm\}$. These results are new and are presented here for the first time.

3 Phenomenological results for Higgs and Drell-Yan production

In this section we present phenomenological results for the SM processes discussed in the previous section. We note that this list of (inclusive) processes exhausts the set of SM processes that can be computed using inclusive results for two-to-one processes. All results are obtained using the code `n3lox`s, which is publicly available as a repository at <https://github.com/jubaglio/n3lox>s. We refer to appendix A for a detailed description of how to use the code. We work with $n_f = 5$ massless quark flavors. For the gluon fusion process, we consider an effective coupling of the Higgs boson to gluons in the large m_t limit (heavy top-quark limit, or HTL) [57–60], with the possibility of a Born-improved prediction where the heavy-top quark predictions are rescaled by the exact Born matrix elements at one loop.² In the case of the neutral-current Drell-Yan process, we include non-decoupling top-mass effects due to the axial anomaly [65, 66] and for the rest assume that the top quark is infinitely heavy and its degrees of freedom are integrated out. Unless stated otherwise, we present results for a proton-proton collider with a center-of-mass (c.m.) energy $\sqrt{s} = 13$ TeV, and we use the PDF4LHC15_nnlo_mc

²Note, that we can choose either the on-shell scheme or the $\overline{\text{MS}}$ scheme (marked in the plots in this case) for treating the top-quark mass in the Wilson coefficients [61–64] of the HTL Lagrangian.

set [67]. The cross sections depend on the factorization scale μ_F and the renormalization scale μ_R . The central scale choices for μ_F and μ_R are the following:

- $\mu_R^0 = \mu_F^0 = Q$ for Drell-Yan processes, Q being the off-shellness of the intermediate vector boson,
- $\mu_R^0 = \mu_F^0 = \frac{1}{2}m_H$ for Higgs production in gluon fusion,
- $\mu_R^0 = m_H, \mu_F^0 = \frac{1}{4}(m_H + 2m_b)$ for Higgs production in bottom-quark fusion.

The strong coupling is evolved from $\alpha_S(m_Z) = 0.118$ using the five-loop QCD beta function [68–71] in the $\overline{\text{MS}}$ -scheme using $N_f = 5$ active massless quark flavors. For all other numerical input parameters (e.g., electroweak coupling constant, quark and boson masses, etc.) we refer to appendix B. Some of the results discussed in this section have already appeared earlier in the literature [1, 9, 16–18, 22]. We reproduce them here as an illustration and validation of the results one can obtain with `n3lox`s. We will also perform an extensive study of the various sets of parton distribution functions (PDFs), including the latest sets that have been released and for which no results can be previously found in the literature.

3.1 Scale dependence and scale uncertainties

In fig. 2 we show the dependence of the cross section for Higgs production in bottom or gluon fusion on one of the two perturbative scales μ_F or μ_R , with the other held fixed to the corresponding central value. The bands are obtained by varying the fixed scale up and down by a factor of two around its central value. We note that the scale dependence for Higgs production in bottom or gluon fusion at N³LO had already been considered in refs. [1, 9, 18], and we reproduce those results perfectly. This serves as a validation of the code `n3lox`s.

We also present the scale dependence of Drell-Yan processes, i.e., the variation of the cross section when both the perturbative scales μ_F and μ_R are varied by a factor of two around the central scales (μ_F^0, μ_R^0) while respecting the constraint

$$\frac{1}{2} \leq \frac{\mu_R}{\mu_F} \leq 2. \quad (9)$$

Commonly, this is referred to as 7-point variation. The results are given in figs. 3, 4 and 5 where we show the invariant-mass distribution of the neutral- and charged-current Drell-Yan cross sections normalized to the N³LO result as a function of the invariant mass Q of the produced lepton pair with $40 \text{ GeV} \leq Q \leq 180 \text{ GeV}$. For a 13 TeV pp collider, we reproduce the results of refs. [16, 17, 22]. Just like in those references, we observe that for the range of invariant masses considered, the bands from the scale variation do not overlap between NNLO and N³LO. We plot the scale dependence also for $\sqrt{s} = 1.96, 7,$ and 100 TeV, both for pp and $p\bar{p}$ collisions. Even at 100 TeV, where, as expected, the scale variation bands are significantly wider than at 13 TeV, there is no overlap between

the NNLO and N³LO predictions at large Q values. At the Tevatron energy of 1.96 TeV, we note that the NNLO and N³LO bands cross within the plotted range, and thus the non-overlapping bands appear at small values of Q . We do not observe any significantly different behavior between the pp and $p\bar{p}$ colliders.

Figure 6 shows the ratio of the production cross section for a pp and $p\bar{p}$ collider for $\sqrt{s} = 13$ TeV. The neutral- and charged-current processes show a distinct dependence on Q , but the higher-order corrections do not change this behavior qualitatively. Only for the production of an $e^+\nu_e$ pair, the pp collider leads to higher values of the cross section than for the $p\bar{p}$ collisions, and this process shows non-monotonic dependence on the invariant mass Q .

To better understand the perturbative behavior, we plotted in figs. 7, 8 and 9 the individual channels contributing to the NNLO and N³LO cross sections, for 1.96 TeV Tevatron, 13 TeV LHC, and 100 TeV pp and $p\bar{p}$ colliders. We observe substantial, $\mathcal{O}(10)$, cancellations at NNLO for the LHC and 100 TeV collider over large range of Q^2 . The cancellations are substantially less prominent at N³LO, but nevertheless present. They introduce an enhanced sensitivity to the PDFs associated with the cancelling channels. For example, if the combination of PDFs associated with a large, positive channel is slightly varied and the combination associated with a large, negative channel remains the same, the effect of the change in PDFs is enhanced in the prediction of the cross section. If this effect is not accidental, the question arises if it is adequately taken into account at N³LO, because our PDFs are currently extracted at NNLO. Furthermore, the uncertainty of our knowledge of PDFs may give rise to varying cancellation patterns. Note that the definition of the different partonic channels depends on the scheme used to define the PDFs (and all available NNLO PDF sets are defined in $\overline{\text{MS}}$ -scheme), and so the pattern of cancellations may itself be scheme-dependent. If indeed this cancellation has an origin in our current definition of PDFs, we may ask if a more judicious choice of PDF scheme would give rise to an improved description. The points raised above may be part of the answer to the question of why N³LO corrections for Drell-Yan processes are partly not contained within NNLO scale uncertainties.

3.2 PDF study for Drell-Yan and Higgs processes

Given the smallness of the scale uncertainties at N³LO (and already at NNLO for Drell-Yan processes), the dependence of the cross sections on the PDFs becomes the dominant source of theoretical uncertainties at hadron colliders. It is therefore highly desirable to perform a comprehensive study of the various PDF sets available on the market. Indeed, since PDFs need to be extracted from experiment, their value and uncertainty depend on the experimental data used in the fit as well as on the fitting methodology used by the different groups.

Our default set is PDF4LHC15_nnlo_mc (PDF4LHC15) [67], and in addition we have calculated predictions for Drell-Yan and Higgs production processes using the latest updates of the global sets available in 2022:

- The MSHT20 update of MMHT14: MSHT20nnlo_as118 (MSHT20) [72];

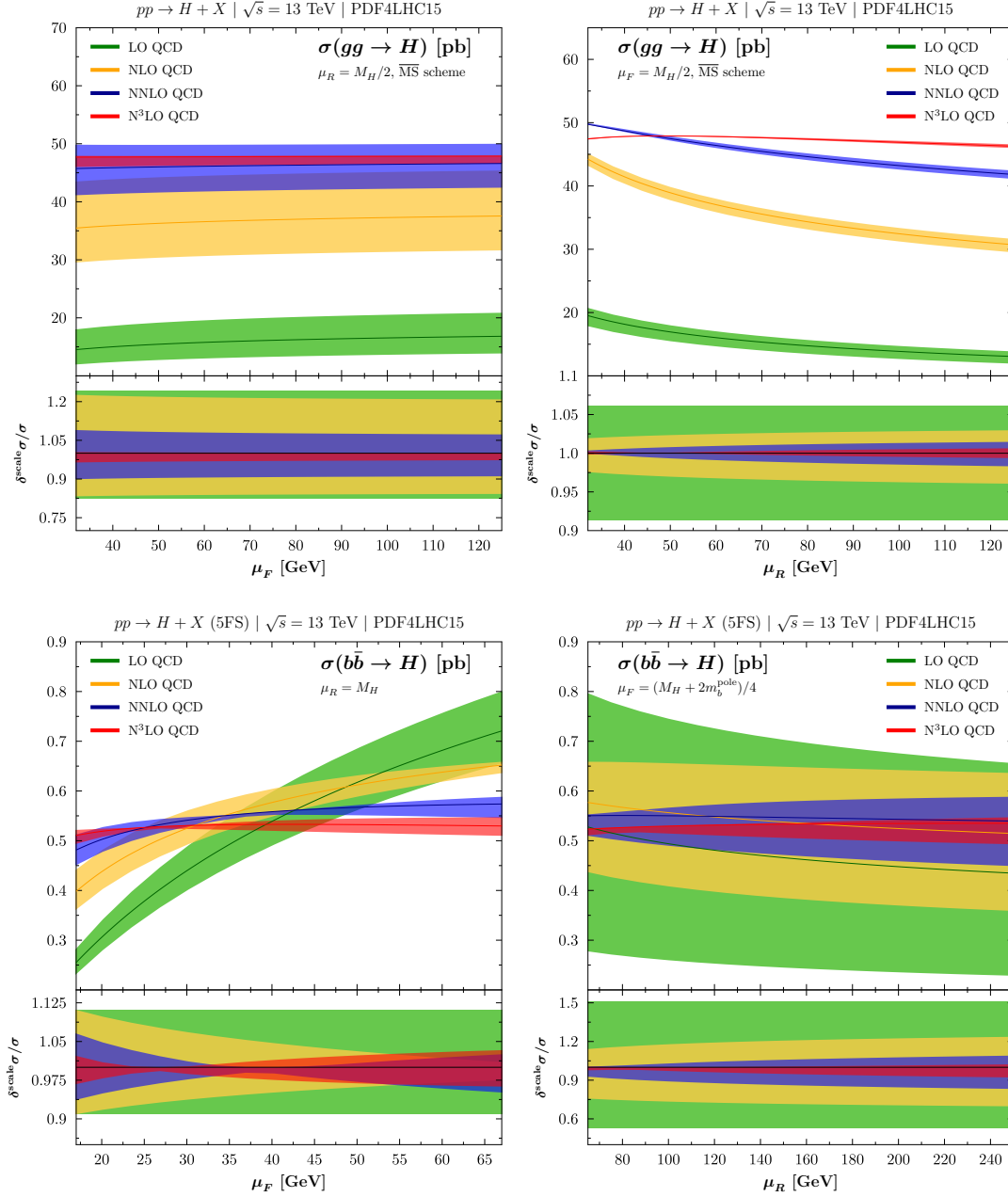


Figure 2: Scale dependence for Higgs production in gluon fusion (upper row) and $b\bar{b}$ annihilation (lower row) at the 13 TeV LHC. The sub-panels display the ratio of the predictions to the central prediction for $\mu_R = \mu_R^0$, $\mu_F = \mu_F^0$. The left panels display the dependence over the factorization scale μ_F while the renormalization scale μ_R is fixed to μ_R^0 , the right panels display the dependence over μ_R while μ_F is fixed to μ_F^0 . Bands represent the variation of the respective other scale by a factor of two up and down w.r.t. its central value.

- The CT18 update from the CTEQ-TEA collaboration, superseding the CT14 global analysis: CT18NNLO (CT18) [73];
- The two last updates from the NNPDF collaboration: NNPDF31_nnlo_as_0118 (NNPDF 3.1) [74] and the latest set NNPDF40_nnlo_as_01180 (NNPDF 4.0) [75];
- The PDF4LHC21 update of PDF4LHC15, based on the statistical Monte-Carlo combination of the three global sets NNPDF 3.1, MSHT20, and CT18: PDF4LHC21_mc [76];
- The last update from the ABMP collaboration: ABMP16als118_5_nnlo (ABMP16_als118) [77].

Each PDF set also includes a fitted value for the input strong coupling constant, $\alpha_S(m_Z)$. It is well known that the ABMP fitted value for this physical parameter is smaller than what is obtained in the other sets that we consider. This has in particular a strong impact on the predictions for Higgs production in gluon fusion. Since ABMP16 also contains PDF sets with alternative fitted values for $\alpha_S(m_Z)$, we have chosen to select the one which uses $\alpha_S(m_Z) = 0.118$ as in the other sets. This greatly improves the agreement between e.g. PDF4LHC15 and ABMP16 predictions for the inclusive $gg \rightarrow H$ hadronic cross section at the LHC.

In figs. 10, 11, 12, 13, and 14, we show the dependence of the Higgs and Drell-Yan cross sections on the choice of the PDF set. We normalize all our results to the central PDF4LHC15 set. The first panel shows a comparison to the PDF4LHC21 set, the second panel shows a comparison to the NNPDF 3.1 and NNPDF 4.0 sets. For all these sets the PDF uncertainties have been computed using the Monte-Carlo replica method adapted to produce a 68% CL uncertainty, following the prescription of ref. [67]. The lower panels show results with ABMP16_als118, CT18, and MSHT20 sets. The PDF uncertainties for these sets have been evaluated using the Hessian prescription rescaled to 68% CL (1σ , assuming a Gaussian distribution) when needed (this is the case for CT18 which provides error sets for 90% CL Hessian errors). Note that the PDF uncertainty for the MSHT20 PDF set is asymmetric. We observe that various sets show overall rather good agreement with one another (up to some deviations which we will highlight below), and that CT18 always provides the largest PDF uncertainty amongst the newest sets. Nonetheless, the systematic bias introduced by a specific choice of PDF set can be substantial, and we observe large variations in the width of the error bands for different sets.

In the case of gluon fusion Higgs production, all sets are in agreement, as seen in fig. 10, and apart from CT18, all newer sets give smaller PDF uncertainties compared to PDF4LHC15. This process is more sensitive to the input value of $\alpha_S(m_Z)$ than to the PDFs themselves. Indeed, while we observe a good agreement between ABMP16_als118 and PDF4LHC15, this would not have been the case between PDF4LHC15 and the nominal ABMP16 PDF set which has a lower fitted value of $\alpha_S(m_Z)$.

There is a spectacular reduction of the PDF uncertainties for bottom-quark fusion Higgs production as seen in fig. 11, with all new sets giving substantially smaller uncertainties compared to the nominal PDF4LHC15 set. The central value also shifted

noticeably. This reflects a strong improvement in the determination of the bottom-quark PDF in the newest sets. For c.m. energies above 50 TeV, ABMP16_als118 and PDF4LHC15 display a 1σ disagreement, while for low c.m. energies below 10 TeV there is also at least 1σ deviation between both NNPDF sets and PDF4LHC15.

The study of the Drell-Yan processes is very interesting, as they are standard candle processes at hadron colliders. In the case of neutral Drell-Yan production, displayed in fig. 12, PDF4LHC21 has smaller uncertainties at values of the invariant mass Q below 600 GeV, but larger uncertainties for $Q > 600$ GeV. All sets but CT18 display a similar downward trend when going to larger values of Q , and more interestingly the newest NNPDF 4.0 set is in disagreement with PDF4LHC15 at the 1σ level for $Q < 600$ GeV, and in particular around the Z peak where it also disagrees with NNPDF 3.1. In the case of charged-current W^+ production, displayed in fig. 13, both NNPDF sets show significant differences, at the 1σ level, for Q values between 200 and 600 GeV. The deviation extends up to Q values of around 1250 GeV for NNPDF 4.0. The case of W^- production cross sections, shown in fig. 14, displays significant differences in large Q^2 ranges between the older set and the newer updates. The NNPDF and PDF4LHC sets show a significant shift toward the ABMP16_als118 results for this process. The latter, in particular, is in significant disagreement with PDF4LHC15 predictions for $Q > 600$ GeV, beyond the 1σ level. Again NNPDF 4.0 is in a 1σ disagreement with PDF4LHC15 (and PDF4LHC21) for low Q values below 200 GeV and in particular around the W peak. This behavior signals a systematic trend in all Drell-Yan processes that calls for further investigations to understand why these differences exist in this particular set.

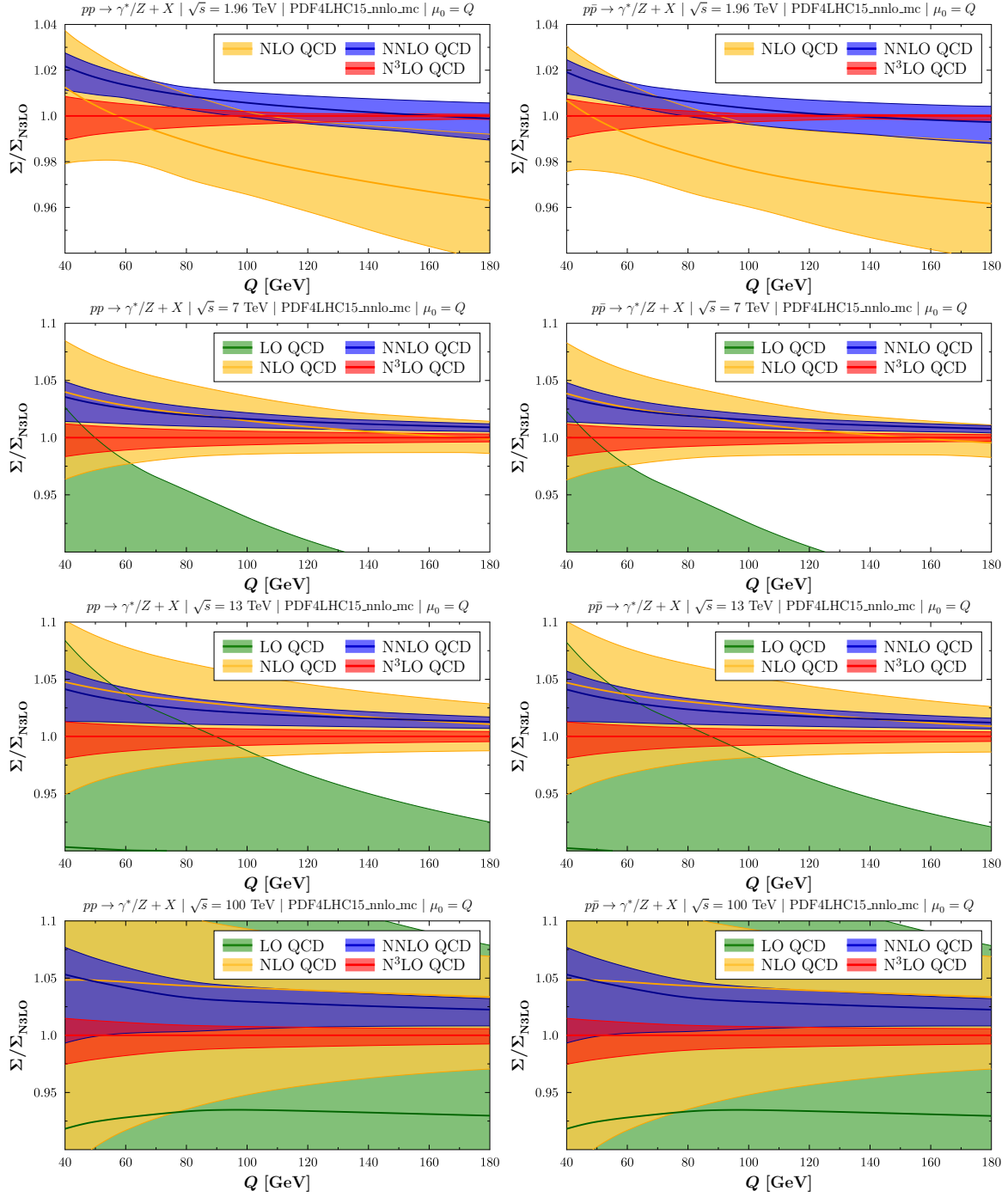


Figure 3: Dependence of the neutral-current γ/Z Drell-Yan cross sections on the invariant mass Q of the lepton pair in the final state (in GeV) normalized to the $N^3\text{LO}$ cross section at various center of mass energies for the pp (left column) and $p\bar{p}$ collisions (right column). The bands indicate the 7-point scale uncertainty at each corresponding perturbative order.

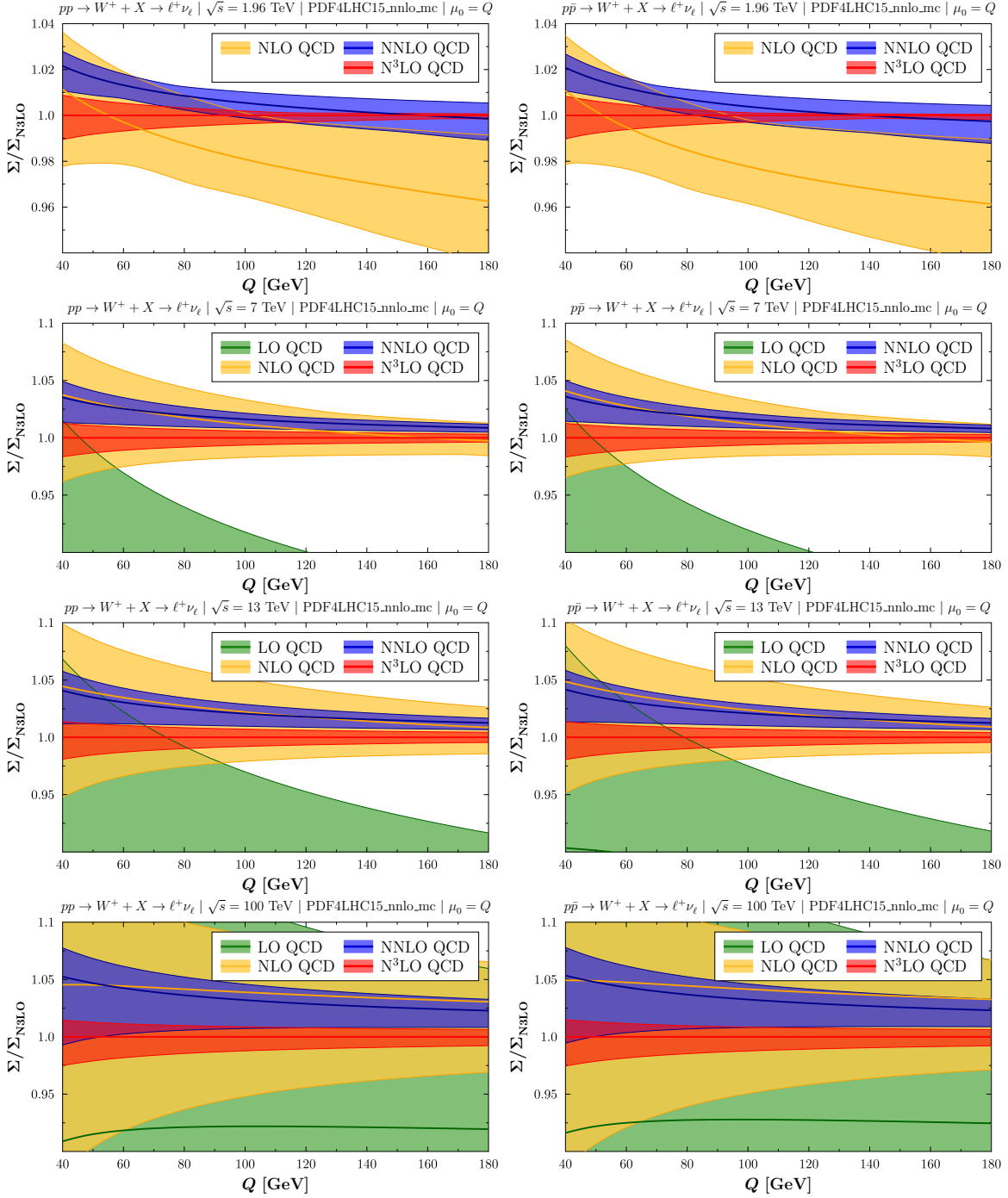


Figure 4: Same as figure 3, but for W^+ production.

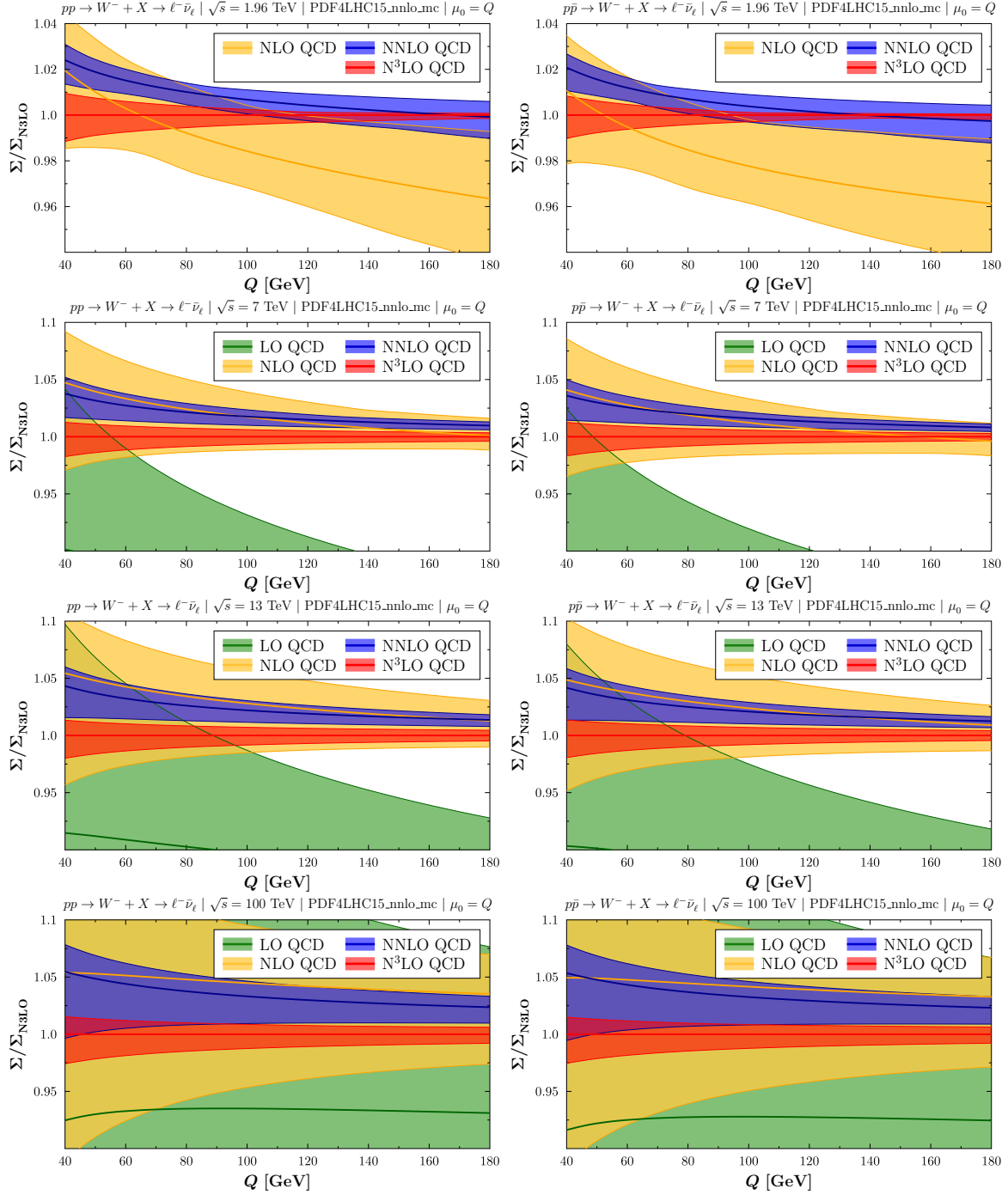


Figure 5: Same as figure 3, but for W^- production.

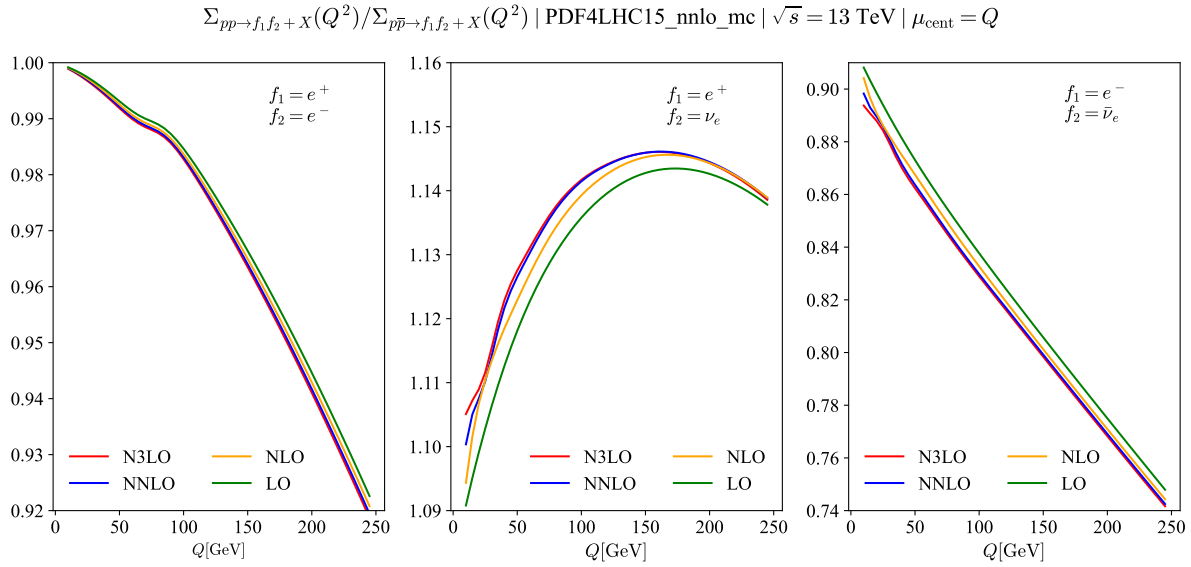


Figure 6: Ratio of the proton-proton to the proton-anti-proton $\Sigma_{pp}^{\text{N}^k\text{LO}}(Q^2) / \Sigma_{p\bar{p}}^{\text{N}^k\text{LO}}(Q^2)$ production cross sections for Drell-Yan processes.

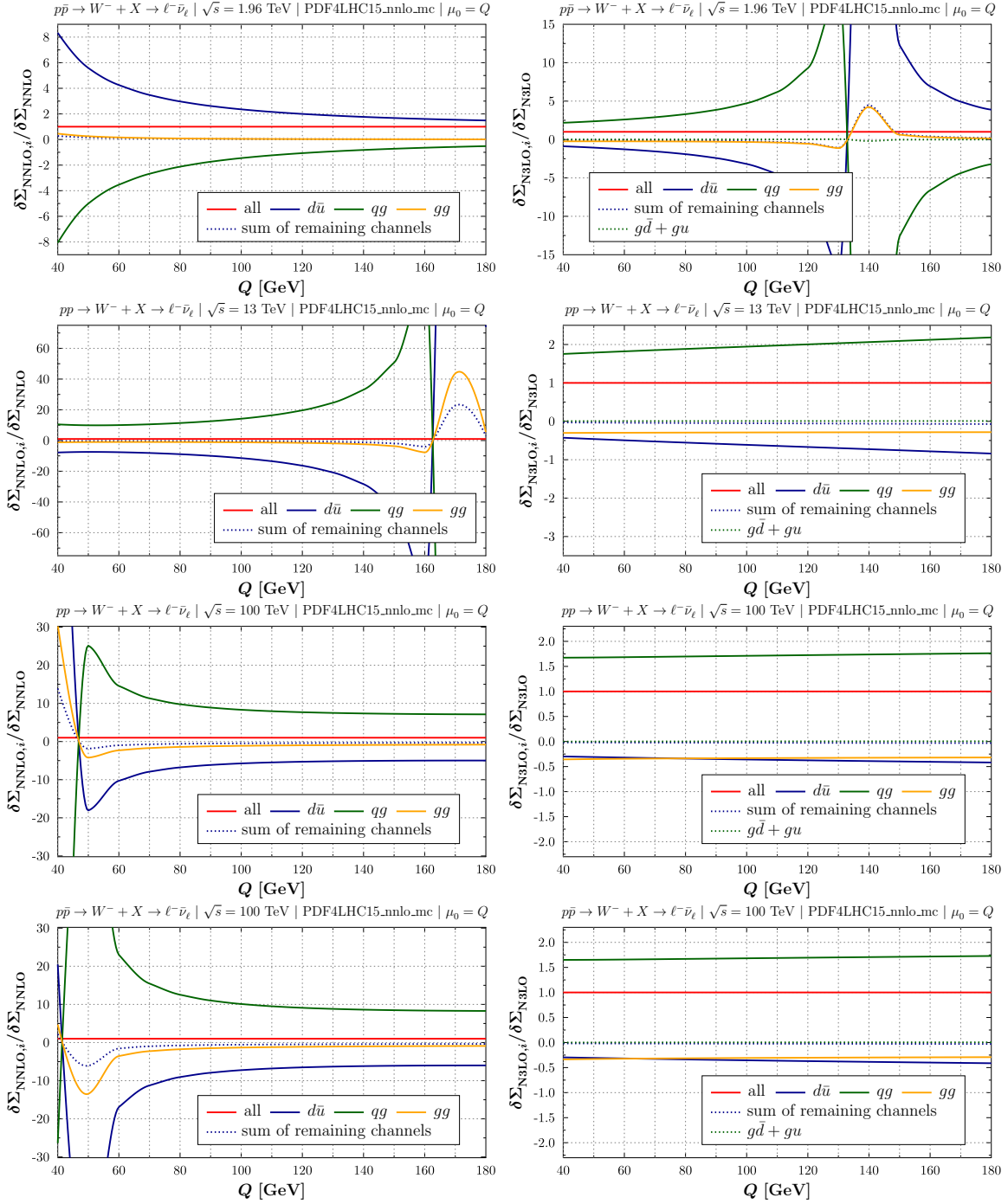


Figure 7: Individual channels contributing to the invariant mass distribution for the production of an $e^- \bar{\nu}_e$ pair at different colliders, normalized to the total correction at NNLO (left panels) and N³LO (right panels).

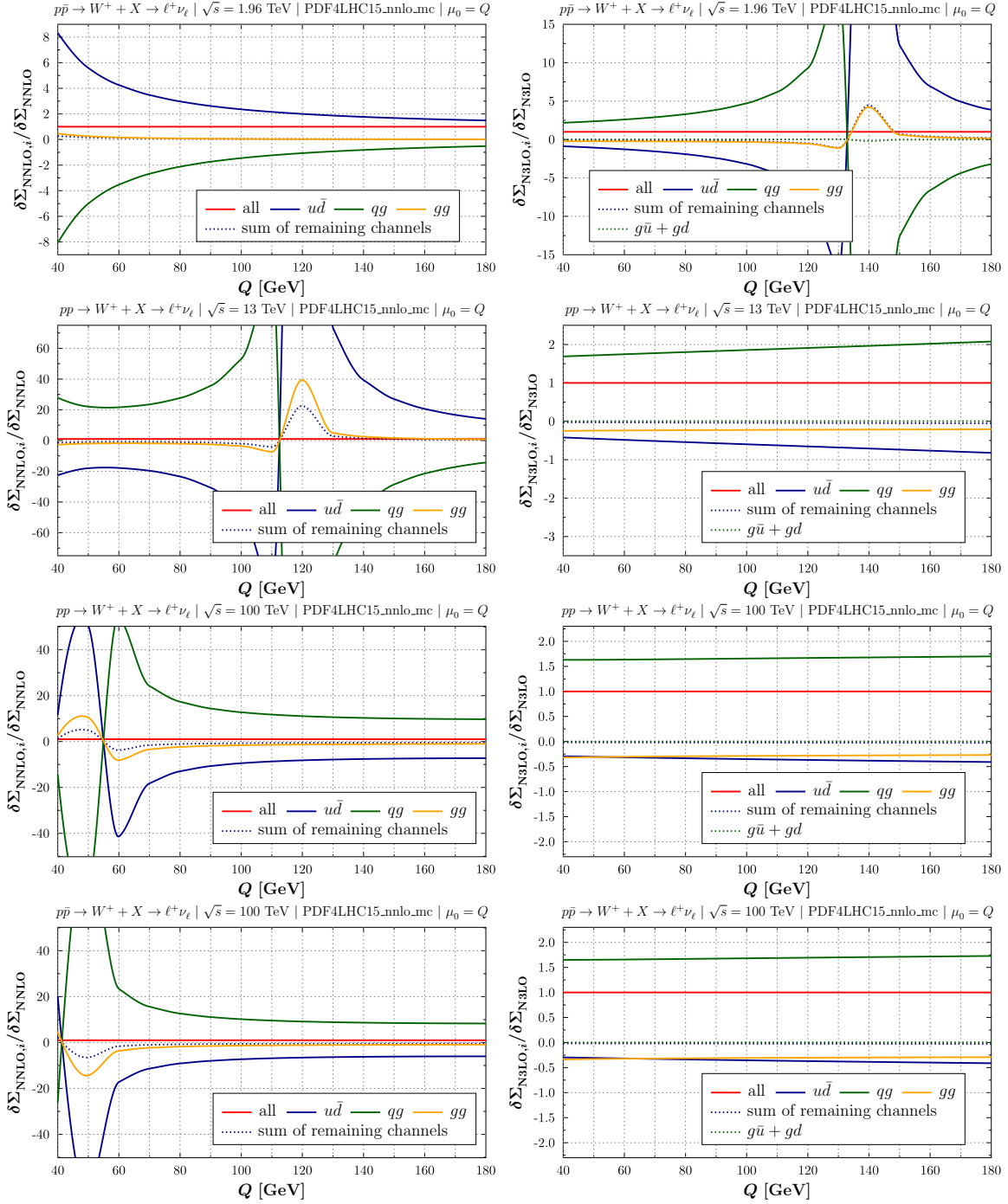


Figure 8: Individual channels contributing to the invariant mass distribution for the production of an $e^+\nu_e$ pair at different colliders normalized to the total correction at NNLO (left panels) and N³LO (right panels).

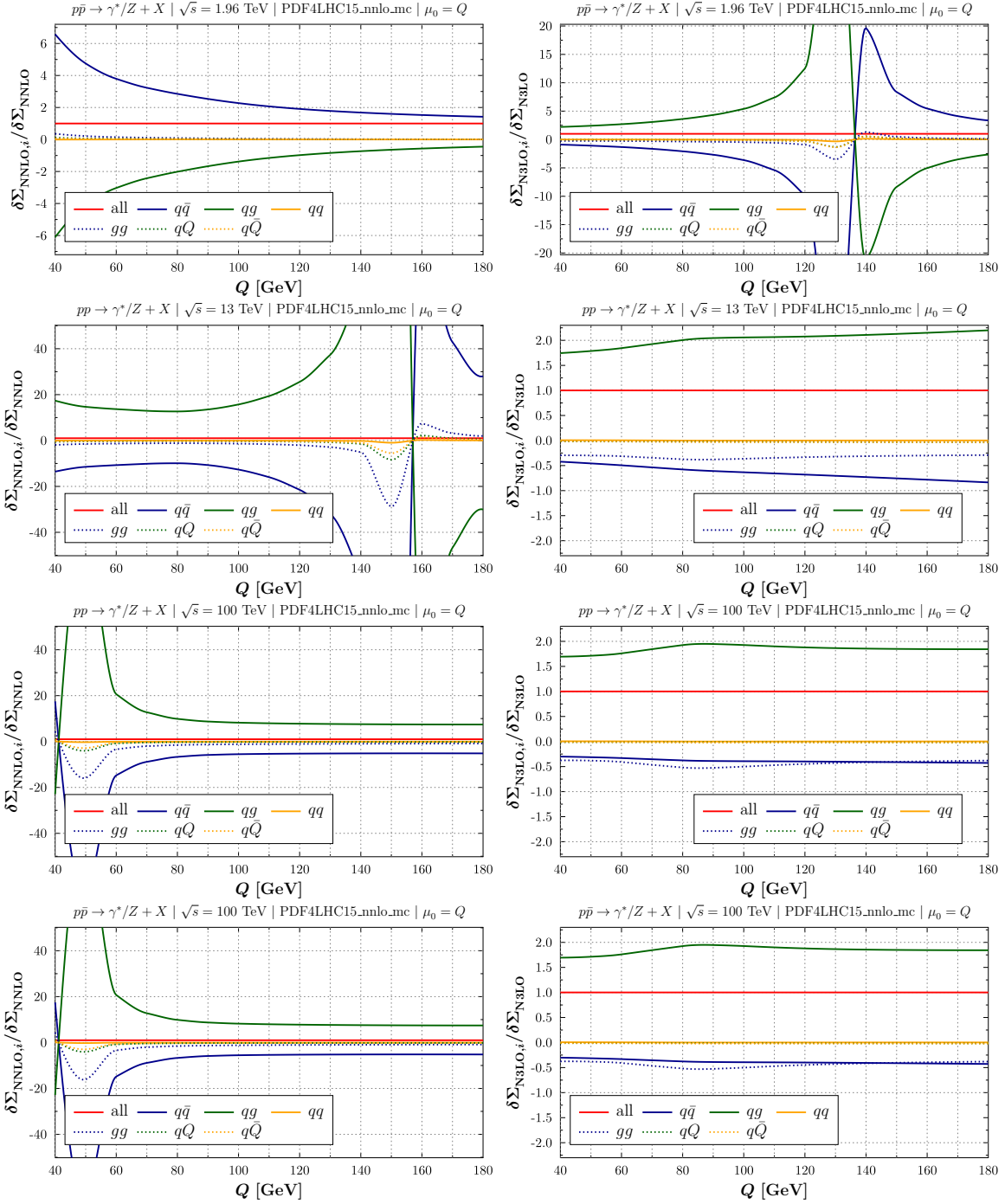


Figure 9: Individual channels contributing to the invariant mass distribution for the production of an e^+e^- pair at different colliders normalized to the total correction at NNLO (left panels) and N³LO (right panels).

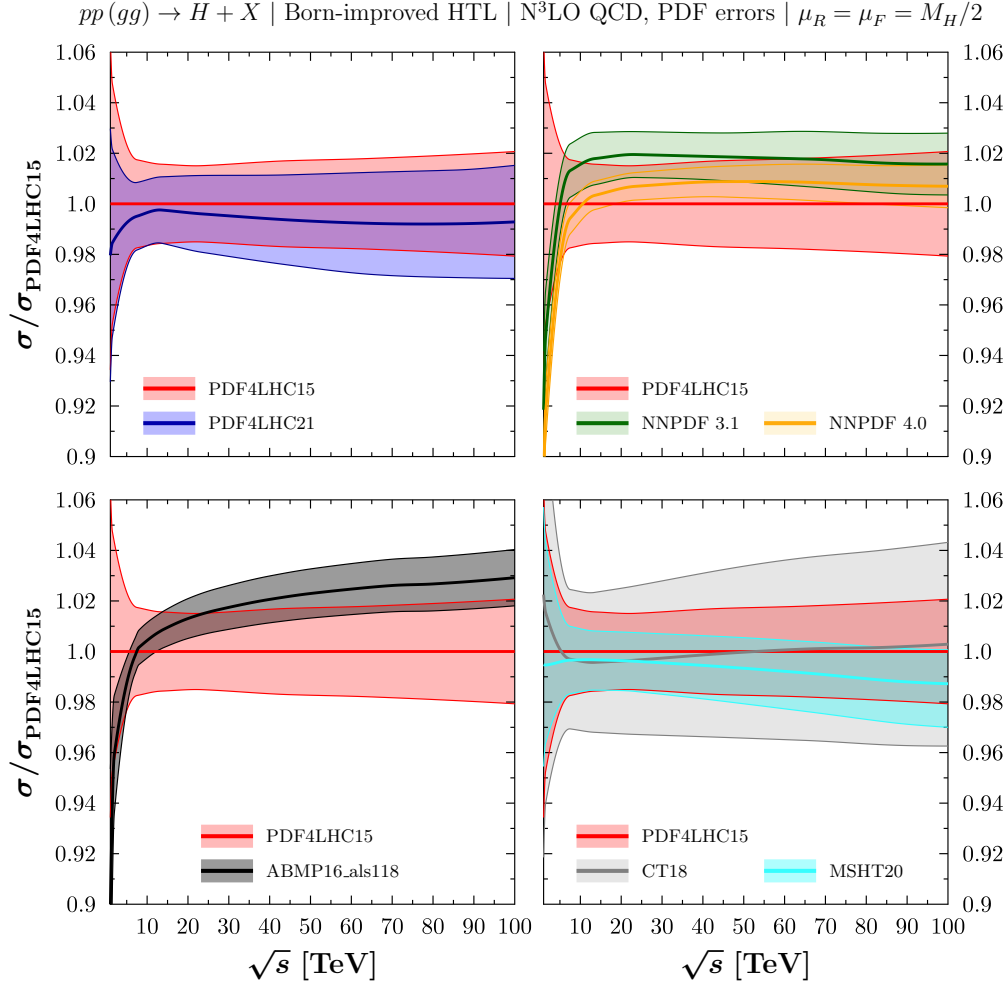


Figure 10: Dependence on the choice of the PDF set of the Born-improved HTL gluon fusion Higgs production cross section at N³LO in QCD as a function of the proton-proton c.m. energy \sqrt{s} in TeV. The results are normalized to the central PDF4LHC15 PDF set and the 68% CL PDF uncertainties are represented by bands for all sets and calculated according to the prescription of ref. [67]. The comparison is between PDF4LHC15 and: PDF4LHC21 (upper left panel); NNPDF 3.1 and NNPDF 4.0 (upper right panel); ABMP16_als118 (lower left panel); CT18 and MSHT 20 (lower right panel).

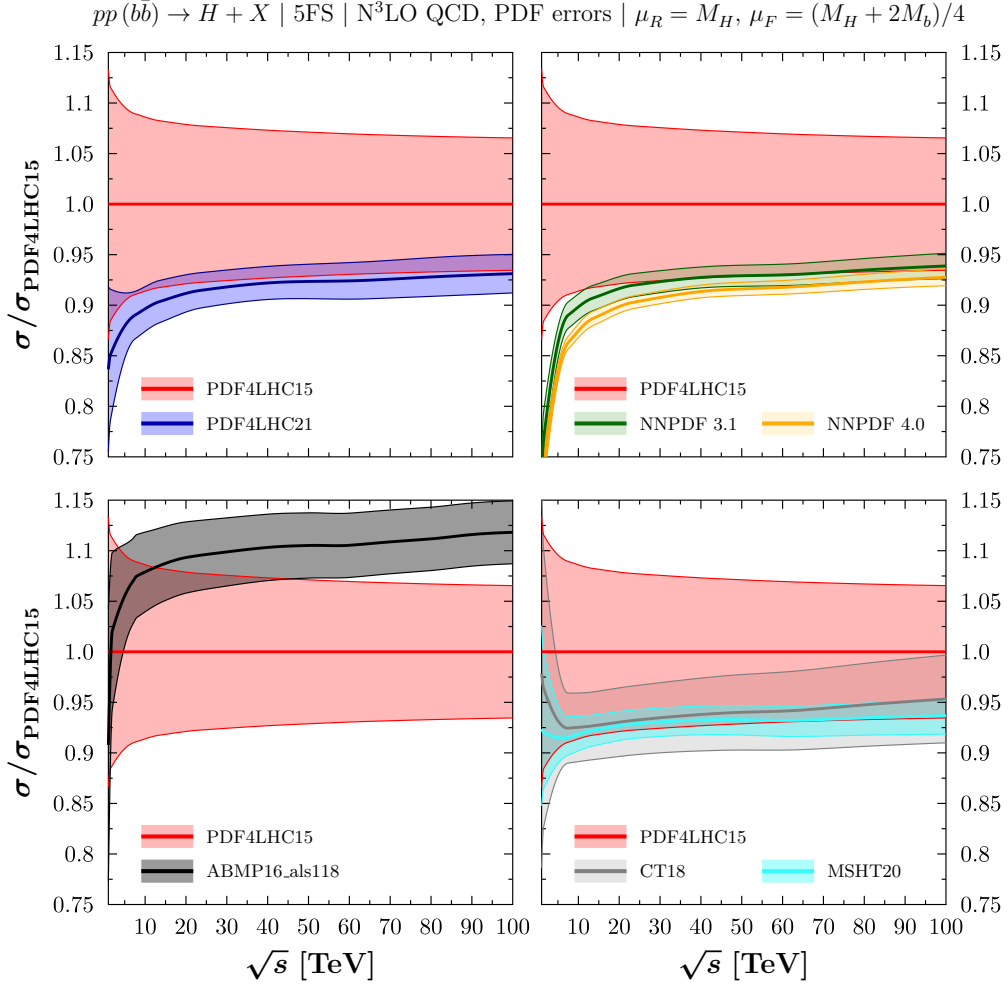


Figure 11: Same as in fig. 10, but for bottom-quark-fusion Higgs production in the five-flavor-scheme.

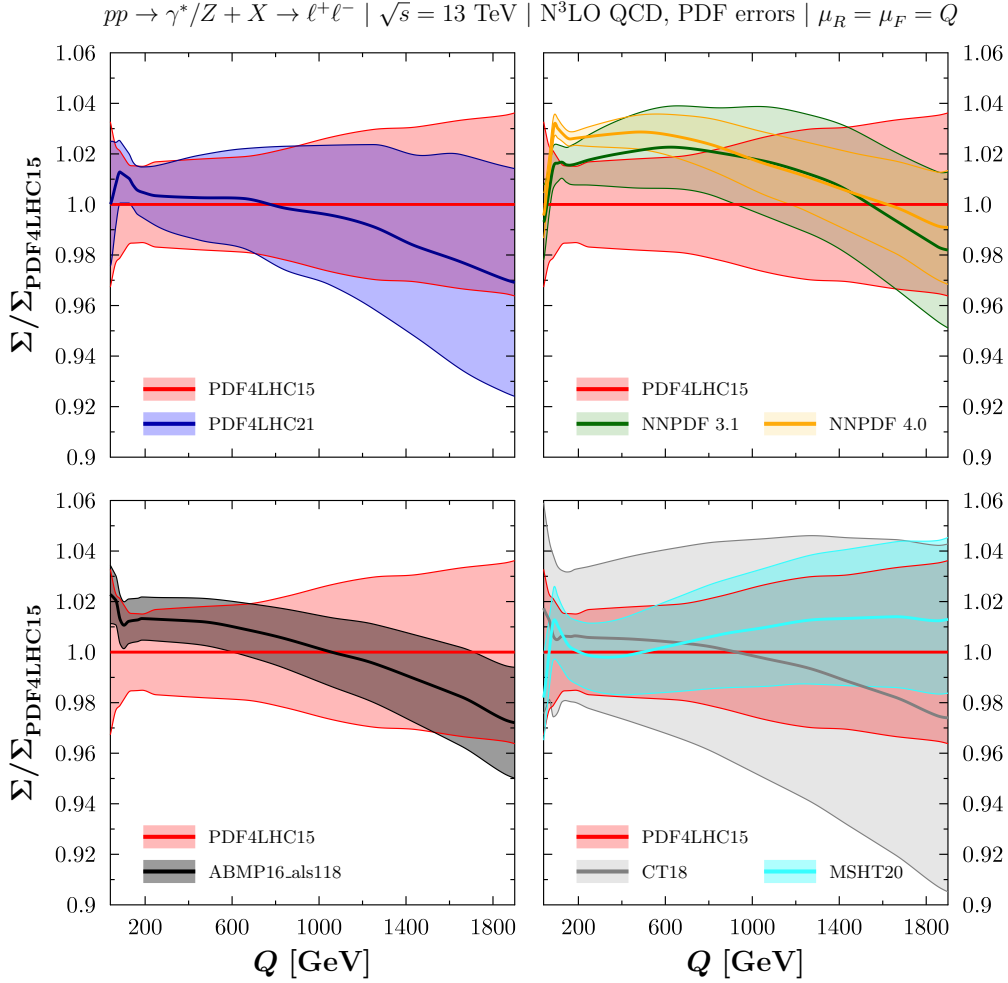


Figure 12: Dependence on the choice of the PDF set of the neutral-current Drell-Yan differential cross section at N³LO in QCD as a function of the invariant mass Q of the final-state lepton pair, at the 13 TeV LHC. The results are normalized to the central PDF4LHC15 PDF set and the 68% CL PDF uncertainties are represented by bands for all sets and calculated according to the prescription of ref. [67]. The comparison is between PDF4LHC15 and: PDF4LHC21 (upper left panel); NNPDF 3.1 and NNPDF 4.0 (upper right panel); ABMP16_als118 (lower left panel); CT18 and MSHT 20 (lower right panel).

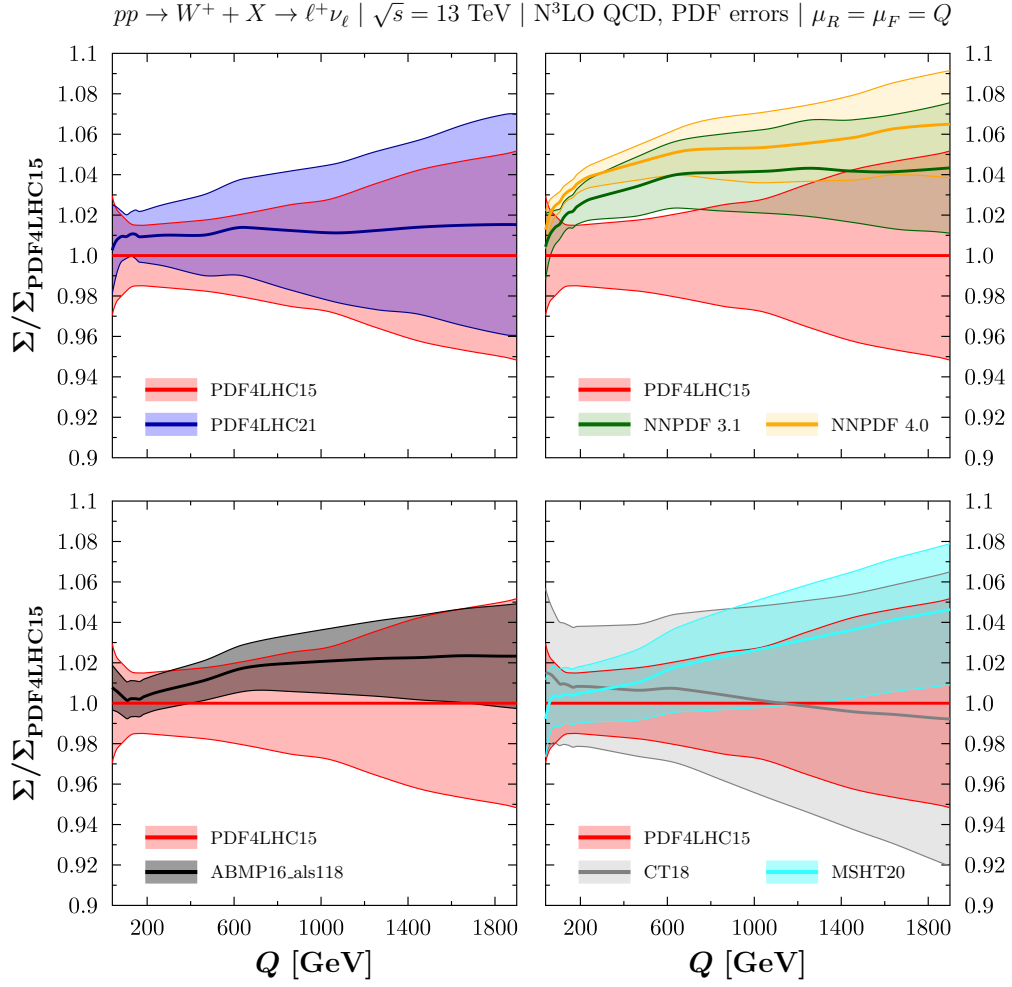


Figure 13: Same as in fig. 12, but for charged-current W^+ Drell-Yan differential cross section.

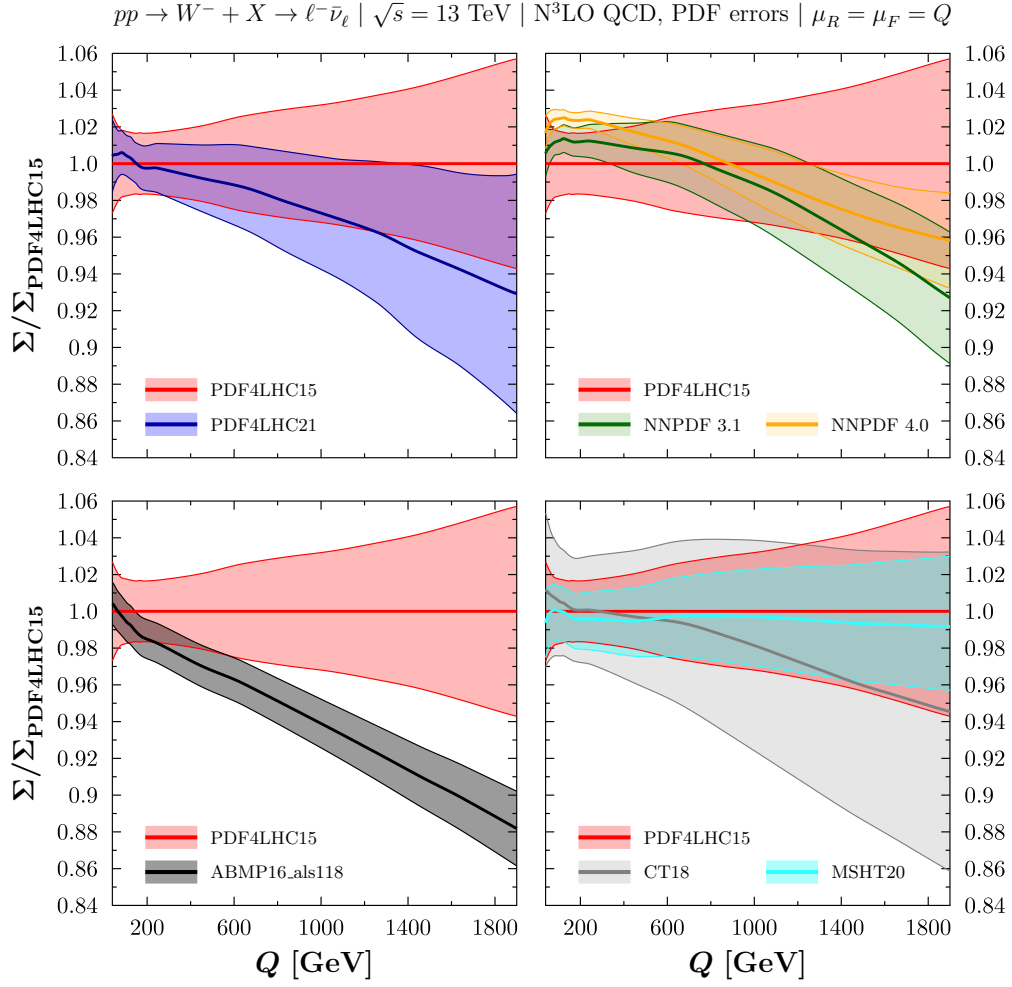


Figure 14: Same as in fig. 12, but for charged-current W^- Drell-Yan differential cross section.

4 Inclusive associated VH production at N³LO

In this section, we present for the first time results for the fully inclusive cross section at N³LO for the production of a Higgs boson in association with a weak boson $V = Z, W^\pm$ in QCD with $N_f = 5$ massless flavors. We only include Drell-Yan-like contributions, i.e. the diagrams where the Higgs boson couples directly to the intermediate vector boson.³ The NLO QCD corrections were evaluated in refs. [87–89], while the NNLO QCD corrections were given in ref. [90] for the inclusive cross section and have been implemented in the code `vh@nnlo` [91, 92]. The NNLO QCD corrections have also been extended to exclusive cross sections and fully differential observables in refs. [93, 94], and later also to include the Higgs decays in refs. [95–98]. An NNLO QCD analysis with a resolved jet was performed in refs. [99, 100]. The NLO electroweak corrections are also known [101, 102] and are rather sizeable.

The Drell-Yan-like contribution comes from the virtual vector boson V^* exchanged in the s -channel and its subsequent splitting into Higgs and on-shell V boson. We can obtain this cross section by integrating the invariant-mass distribution in eq. (2) over the virtuality of the intermediate off-shell vector boson:

$$\begin{aligned} \sigma_{N_1 N_2 \rightarrow VH} &= \int_{(m_H+m_V)^2}^s dQ^2 \frac{d\sigma_{N_1 N_2 \rightarrow V^*}}{dQ^2} \frac{Q^4}{(Q^2 - m_V^2)^2} \frac{m_V^2}{48\pi^2 v^2} \\ &\times \sqrt{\lambda\left(1, \frac{m_V^2}{Q^2}, \frac{m_H^2}{Q^2}\right)} \left[\lambda\left(1, \frac{m_V^2}{Q^2}, \frac{m_H^2}{Q^2}\right) + 12 \frac{m_V^2}{Q^2} \right], \end{aligned} \quad (10)$$

with the Källén function

$$\lambda(a, b, c) = (a - b - c)^2 - 4bc. \quad (11)$$

The integration over the virtuality can be performed numerically within `n3lox`s (in fact, it can be done for arbitrary invariant mass ranges, see appendix D).

4.1 Inclusive cross sections and scale uncertainties

We now present phenomenological results for the LHC. Unless stated otherwise, we use the same setup as for the results in section 3. In Table 1 we show the total cross section at the LHC with a c.m. energy $\sqrt{s} = 13$ TeV. Additional results for other c.m. energies are provided in appendix C. Uncertainties have been computed using a 7-point scale variation by varying the scales around a fixed central scale $\mu_0 = m_H + m_V$. K-factors, defined as the

³In particular, we neglect contributions to ZH production from box diagrams where the Higgs boson couples to a heavy fermion loop. The LO analysis can be found in ref. [78], the NLO QCD corrections to $gg \rightarrow ZH$ in the heavy-top quark limit can be found in ref. [79] while the NLO QCD corrections (two-loop corrections) including the top-quark dependence have been computed recently, see refs. [80–85]. We also neglect the top-quark radiated contributions to VH calculated in ref. [86], known to be very small for inclusive rates.

Process	σ^{LO} [pb]	σ^{NLO} [pb]	K^{NLO}	σ^{NNLO} [pb]	K^{NNLO}	$\sigma^{\text{N}^3\text{LO}}$ [pb]	$K^{\text{N}^3\text{LO}}$
W^+H	$0.753^{+2.70\%}_{-3.49\%}$	$0.886^{+1.54\%}_{-1.27\%}$	1.18	$0.891^{+0.24\%}_{-0.29\%}$	1.18	$0.883^{+0.29\%}_{-0.34\%}$	1.17
W^-H	$0.480^{+2.79\%}_{-3.63\%}$	$0.562^{+1.49\%}_{-1.23\%}$	1.17	$0.564^{+0.24\%}_{-0.29\%}$	1.17	$0.558^{+0.31\%}_{-0.36\%}$	1.16
ZH	$0.673^{+2.66\%}_{-3.44\%}$	$0.788^{+1.48\%}_{-1.23\%}$	1.17	$0.792^{+0.22\%}_{-0.27\%}$	1.18	$0.785^{+0.28\%}_{-0.32\%}$	1.17

Table 1: Total cross section for associated Higgs production up to the third-order in perturbation theory at a 13 TeV proton-proton collider for a fixed central scale choice $\mu_0 = m_V + m_H$. The PDF set PDF4LHC15_nnlo_mc has been used for all predictions, and the K-factors, defined as $K^{\text{N}^k\text{LO}} = \sigma^{\text{N}^k\text{LO}}/\sigma^{\text{LO}}$ for $k = 1, 2, 3$, are also given. The quoted uncertainties (in percent) are calculated using a 7-point scale variation around the central scale.

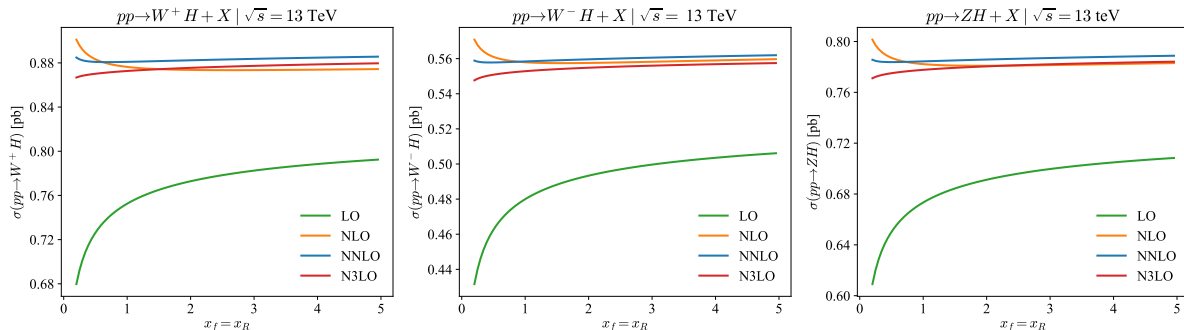


Figure 15: Scale dependence for the associated Higgs production for a fixed central scale choice $\mu_0 = m_V + m_H$. We vary the factorization and renormalization scale in a correlated fashion by varying the parameters x_F and x_R simultaneously (see main text).

ratio between higher-order QCD predictions and LO predictions, $K^{\text{N}^k\text{LO}} = \sigma^{\text{N}^k\text{LO}}/\sigma^{\text{LO}}$ for $k = 1, 2, 3$, are also given. We note that the third-order corrections are larger than the NNLO correction, and that the N^3LO predictions have a slightly larger scale uncertainty (albeit very small, just like at NNLO already). This behavior is analogous to NNLO corrections in the Drell-Yan channels [17, 22], which are based on the same hadronic production cross sections.

Figure 15 shows the dependence of the associated Higgs production on the renormalization and factorization scales set to a common value and varied simultaneously. We defined $x_F = \frac{\mu_F}{\mu_0}$ and $x_R = \frac{\mu_R}{\mu_0}$, with $\mu_0 = m_V + m_H$. Starting from NNLO, we observe that the scale dependence is relatively flat. The corrections for W^\pm and Z exhibit similar dependence. Coincidentally, the N^3LO correction almost entirely cancels with the NNLO contribution for large values of x .

Table 2 contains the total cross sections and the corresponding K-factors for Higgs associated production using a dynamical central scale which is defined in terms of the invariant mass of the VH pair, M_{VH} . Computations are performed again for the a 13 TeV pp (LHC) collider using the PDF4LHC15_nnlo_mc PDF set for all predictions. Typically,

Process	σ^{LO} [pb]	σ^{NLO} [pb]	K^{NLO}	σ^{NNLO} [pb]	K^{NNLO}	$\sigma^{\text{N}^3\text{LO}}$ [pb]	$K^{\text{N}^3\text{LO}}$
W^+H	$0.758^{+2.43\%}_{-3.13\%}$	$0.883^{+1.38\%}_{-1.20\%}$	1.16	$0.891^{+0.28\%}_{-0.34\%}$	1.18	$0.884^{+0.27\%}_{-0.30\%}$	1.17
W^-H	$0.484^{+2.50\%}_{-3.26\%}$	$0.560^{+1.34\%}_{-1.23\%}$	1.16	$0.564^{+0.27\%}_{-0.34\%}$	1.17	$0.559^{+0.30\%}_{-0.33\%}$	1.16
ZH	$0.678^{+2.40\%}_{-3.11\%}$	$0.786^{+1.33\%}_{-1.16\%}$	1.16	$0.792^{+0.25\%}_{-0.32\%}$	1.17	$0.786^{+0.26\%}_{-0.29\%}$	1.16

Table 2: Same as in Table 1, but for a dynamical central scale choice $\mu_0 = M_{VH}$.

when comparing Tables 1 and 2, both scale choices lead to comparable values of the cross section, with the dynamical scale giving slightly smaller scale uncertainties. Similar to the fixed scale choice, the scale uncertainty is not decreasing when going from NNLO to N³LO and stays quite the same. We also present in fig. 16 the predictions for the inclusive cross section as a function of the c.m. energy at a proton-proton collider, including the 7-point scale uncertainties. We noted before that the NNLO and N³LO bands do not overlap for the Drell-Yann processes. As we calculate DY-type contributions to associated Higgs production, this behavior is expected to follow what has already been observed in DY processes.

4.2 Study of the PDF sets and associated PDF, PDF+ α_S and PDF-TH uncertainties

We have also performed an extensive study of the various predictions using different PDF sets, including the 68% confidence level (CL) PDF uncertainties calculated using the prescription associated with each PDF set, see ref. [67] for more details. We use the same PDF sets as in section 3: our default set PDF4LHC15_nnlo_mc (PDF4LHC15) [67], against which we compare its latest update PDF4LHC21_mc (PDF4LHC21) [76], the last MSHT update MSHT20nnlo_as118 (MSHT20) [72], two NNPDF sets NNPDF31_nnlo_as_0118 (NNPDF 3.1) [74] and the latest NNPDF40_nnlo_as_01180 (NNPDF 4.0) [75], as well as CT18NNLO (CT18) [73] and ABMP16als118_5_nnlo (ABMP16_als118) [77]. Note again that the ABMP set we have chosen is not the nominal set, but the one in which $\alpha_S(m_Z) = 0.118$, thus putting on equal foot all sets with respect to their input value for the strong coupling constant. Figures 17, 18, and 19 display the PDF uncertainties for the associated Higgs production with a W^+ , W^- , and Z boson respectively, as a function of the c.m. energy in TeV at a proton-proton collider. All N³LO QCD predictions are normalized to the N³LO QCD result using the central PDF4LHC15 set. We note an overall good agreement between the different PDF sets, though the NNPDF sets show about 1σ deviation in the range of energies relevant for the LHC when compared to the PDF4LHC15 set. This is a reflection of what has been observed for Drell-Yann processes in section 3.2. Except for very low energies, the PDF uncertainties are of the order of a few percent, and significantly larger for CT18 set than for all the other sets.

We have also performed a dedicated PDF+ α_S analysis at the 13 TeV LHC with our nominal PDF4LHC15 set. Following the prescription of ref. [67] we can obtain the correlated PDF+ α_S uncertainty on our predictions, using dedicated sets with $\alpha_S^{1\sigma^-}(m_Z) =$

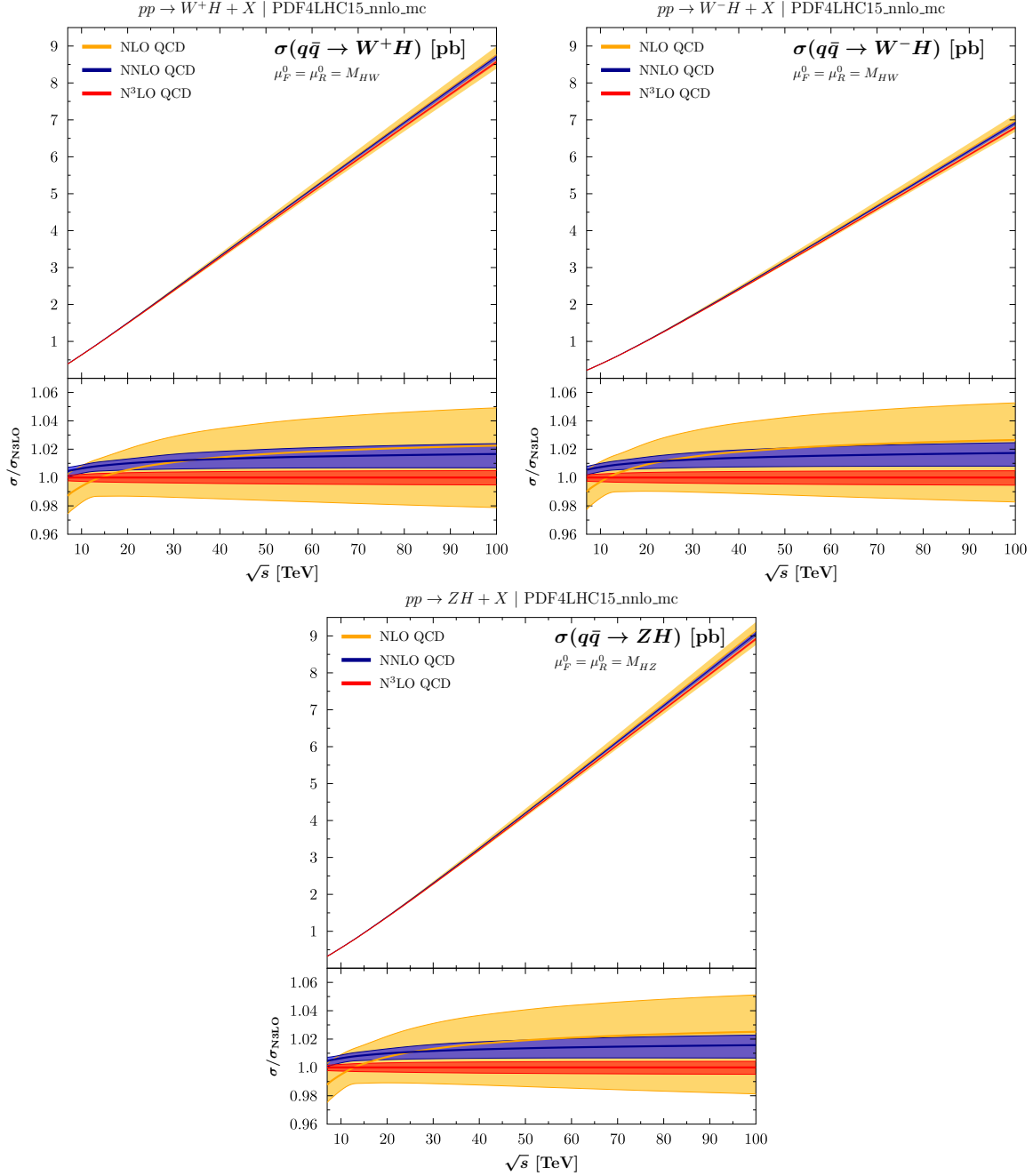


Figure 16: Inclusive cross sections for the associated Higgs production with a massive gauge boson (in pb) at a proton-proton collider as a function of the c.m. energy (in TeV), up to N³LO in QCD including the 7-point scale uncertainty. All cross sections are calculated with the PDF4LHC15_nnlo_mc PDF set. The lower panels display the ratio to the central N³LO prediction. Upper row: $W^\pm H$ predictions. Lower row: ZH predictions.

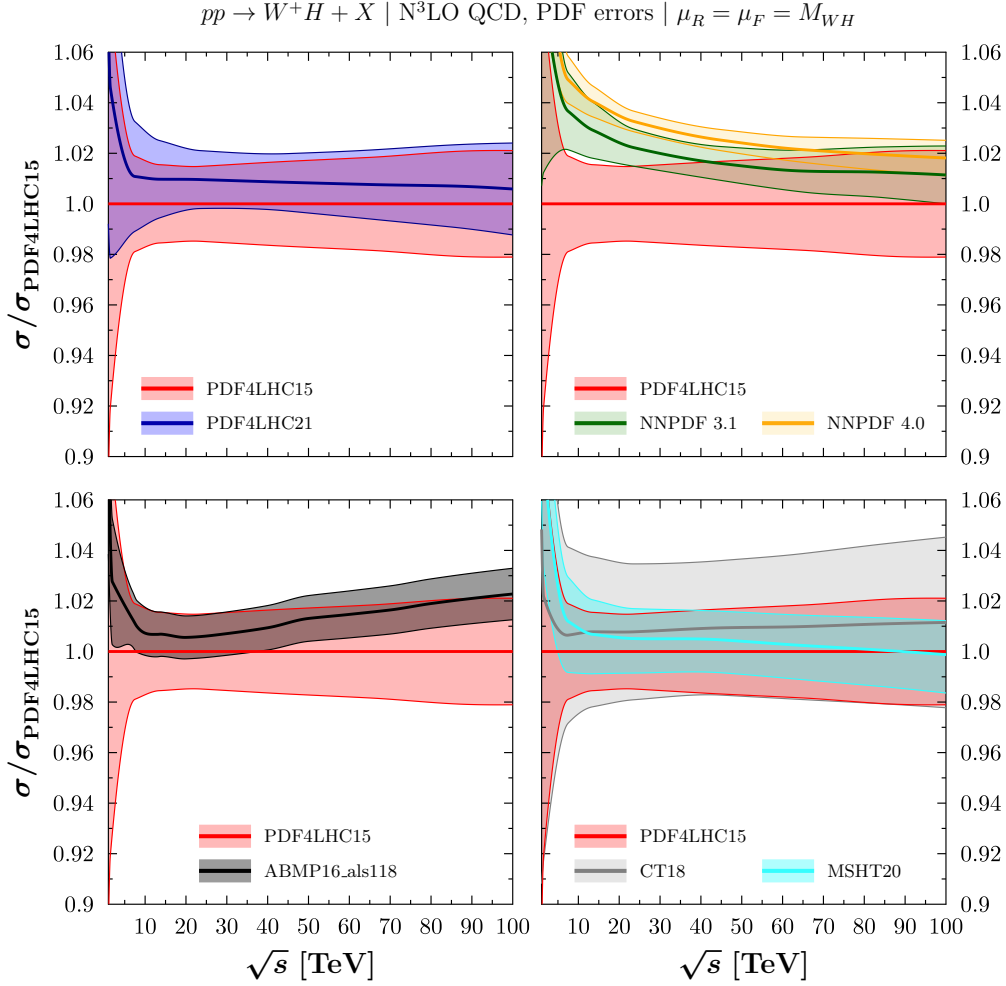


Figure 17: Dependence on the choice of the PDF set of the inclusive cross section at N³LO in QCD, for the associated Higgs production with a W^+ boson at a proton-proton collider using a dynamical central scale, as a function of the proton-proton c.m. energy \sqrt{s} in TeV. The results are normalized to the central PDF4LHC15 PDF set and the 68% CL PDF uncertainties are represented by bands for all sets and calculated according to the prescription of ref. [67]. The comparison is between PDF4LHC15 and: PDF4LHC21 (upper left panel); NNPDF 3.1 and NNPDF 4.0 (upper right panel); ABMP16 als118 (lower left panel); CT18 and MSHT 20 (lower right panel).

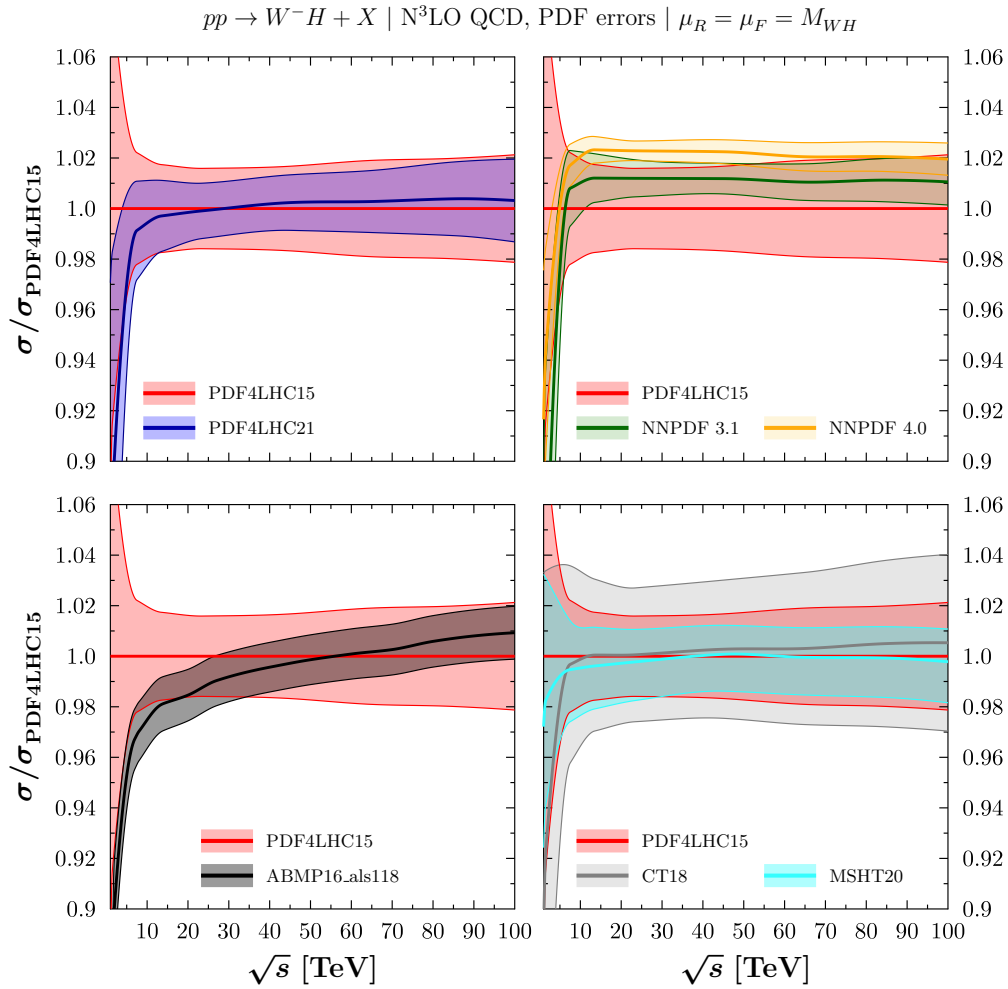


Figure 18: Same as in fig. 17, but for $W^- H$ inclusive cross section.

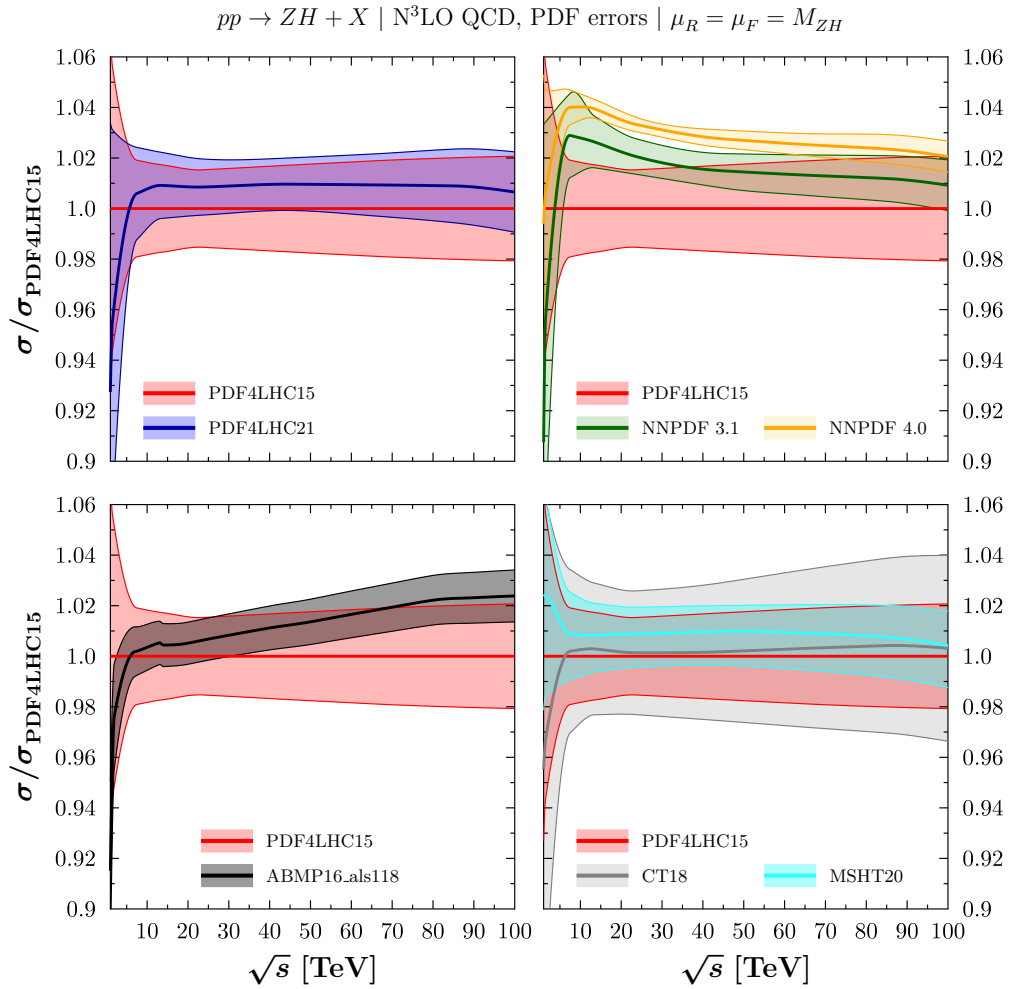


Figure 19: Same as in fig. 17, but for ZH inclusive cross section.

Process	$\sigma^{\text{N}^3\text{LO}}$ [pb]	$\delta(\text{PDF})$ [%]	$\delta(\text{PDF} + \alpha_S)$ [%]	$\delta(\text{PDF-TH})$ [%]
W^+H	0.884	± 1.59	± 1.80	± 1.45
W^-H	0.559	± 1.76	± 1.92	± 1.63
ZH	0.786	± 1.77	± 1.95	± 1.53

Table 3: Total cross section for associated Higgs production at N³LO in QCD, at a 13 TeV pp collider for a dynamical central scale choice $\mu_0 = M_{HV}$. The PDF set PDF4LHC15_nnlo_mc has been used. The symmetrical PDF, PDF+ α_S , and PDF-TH uncertainties (in percent) are also given.

0.1165 and $\alpha_S^{1\sigma^+}(m_Z) = 0.1195$ as lower and upper deviations at 1σ from the central fitted value of the strong coupling constant $\alpha_S(m_Z) = 0.118$. This gives (in percent) the uncertainty

$$\delta(\alpha_S) = \frac{\sigma^{\text{N}^3\text{LO}}(\alpha_S^{1\sigma^+}(m_Z)) - \sigma^{\text{N}^3\text{LO}}(\alpha_S^{1\sigma^-}(m_Z))}{2}, \quad (12)$$

which combined with $\delta(\text{PDF})$ in quadrature gives the uncertainty (in percent) $\delta(\text{PDF} + \alpha_S)$,

$$\delta(\text{PDF} + \alpha_S) = \sqrt{\delta(\text{PDF})^2 + \delta(\alpha_S)^2}. \quad (13)$$

On top of this uncertainty, we have to take into account the mismatch at N³LO between the perturbative order of the hard coefficients (at N³LO), and the perturbative order of the PDFs (at NNLO). As currently no PDF set is obtained using data extracted at N³LO accuracy yet, we can use the prescription introduced in ref. [9] to account for this mismatch and the error induced by the missing accuracy in the PDF determination and calculate a PDF-TH uncertainty $\delta(\text{PDF-TH})$ (in percent). We compare at NNLO the predictions obtained using NNLO and NLO PDF sets, and divide by two the result to account for the fact that the mismatch at N³LO is expected to be smaller than at NNLO,

$$\delta(\text{PDF-TH}) = \frac{1}{2} \frac{|\sigma^{\text{NNLO}}(\text{NNLO PDF}) - \sigma^{\text{NNLO}}(\text{NLO PDF})|}{\sigma^{\text{NNLO}}(\text{NNLO PDF})}. \quad (14)$$

Table 3 displays the predictions obtained at the LHC at 13 TeV for inclusive Higgsstrahlung cross sections with a dynamical central scale. The PDF+ α_S and PDF-TH uncertainties are of comparable size, around $\pm 1.5\%$ to $\pm 2\%$. They are much bigger than the scale uncertainty at N³LO and are the dominant source of theoretical errors at this perturbative order in the QCD expansion. Analogous results for the fixed scale are shown in Table 4. As expected, the choice of the scale has minimal impact on the PDF and α_S uncertainties.

Process	$\sigma^{\text{N}^3\text{LO}}$ [pb]	$\delta(\text{PDF})$ [%]	$\delta(\text{PDF} + \alpha_S)$ [%]	$\delta(\text{PDF-TH})$ [%]
W^+H	0.883	± 1.59	± 1.80	± 1.45
W^-H	0.558	± 1.76	± 1.93	± 1.64
ZH	0.785	± 1.82	± 1.99	± 1.54

Table 4: Total cross section for associated Higgs production at N³LO in QCD, at a 13 TeV pp collider for a fixed central scale choice $\mu_0 = M_V + M_H$. The PDF set PDF4LHC15_nnlo_mc has been used. The symmetrical PDF, PDF+ α_S , and PDF-TH uncertainties (in percent) are also given.

5 Comparison of N³LO predictions

In this paper, we have collected phenomenological predictions for a range of diverse processes computed to N³LO in perturbative QCD. While quantum corrections affect each process in a unique way and their particular form is subject to the kinematic restrictions placed on the process, it is informative to use this range of processes to learn about the qualitative features of perturbative corrections at this order (see also ref. [103]). The processes considered here fall in the category of production processes - two highly energetic initial-state partons undergo a scattering process to produce a specific final state. They are paratypical examples of a much larger range of scattering processes studied at the LHC. The universality of QCD radiation leads us to expect similar features of N³LO corrections in other processes that have not yet been calculated at the same perturbative order. In particular, examples are multi-boson production processes, like the cross section to produce two Z or W bosons.

	Q [GeV]	$\delta\sigma^{\text{N}^3\text{LO}}$	$\delta\sigma^{\text{NNLO}}$	$\delta(\text{scale})$	$\delta(\text{PDF} + \alpha_S)$	$\delta(\text{PDF-TH})$
$gg \rightarrow \text{Higgs}$	m_H	3.5%	30%	+0.21% -2.37%	$\pm 3.2\%$	$\pm 1.2\%$
$b\bar{b} \rightarrow \text{Higgs}$	m_H	-2.3%	2.1%	+3.0% -4.8%	$\pm 8.4\%$	$\pm 2.5\%$
NCDY	30	-4.8%	-0.34%	+1.53% -2.54%	+3.7% -3.8%	$\pm 2.8\%$
	100	-2.1%	-2.3%	+0.66% -0.79%	+1.8% -1.9%	$\pm 2.5\%$
CCDY(W^+)	30	-4.7%	-0.1%	+2.5% -1.7%	$\pm 3.95\%$	$\pm 3.2\%$
	150	-2.0%	-0.1%	+0.5% -0.5%	$\pm 1.9\%$	$\pm 2.1\%$
CCDY(W^-)	30	-5.0%	-0.1%	+2.6% -1.6%	$\pm 3.7\%$	$\pm 3.2\%$
	150	-2.1%	-0.6%	+0.6% -0.5%	$\pm 2\%$	$\pm 2.13\%$

Table 5: Results for production processes obtained with n3loxs. For details, see the discussion in the main text.

In Table 5 we compare predictions for N³LO predictions for Higgs production in gluon- and bottom-quark-fusion and charged- and neutral-current Drell-Yan production.

These processes represent examples of gluon- and quark-induced processes at the LHC. Note that we do not include all available N³LO results for inclusive processes, but we focus on two-to-one inclusive processes at the LHC, which we believe to represent a set of hadron-collider observables that can be compared consistently. In particular, we do not include the VH processes of section 4, because they are based on the same coefficient functions as the Drell-Yan processes. We also do not include the N³LO results for VBF [15, 21], because they are based on DIS coefficient functions, and thus the pattern of QCD corrections is expected to follow the pattern for DIS processes rather than hadron collider processes.

First let us comment on the size of N³LO corrections. We define

$$\delta\sigma_X^{\text{N}^n\text{LO}} = \frac{\Sigma_X^{\text{N}^n\text{LO}}(Q^2)}{\Sigma_X^{\text{N}^{n-1}\text{LO}}(Q^2)} - 1. \quad (15)$$

We observe that for the production processes listed here, $\delta\sigma_X^{\text{N}^3\text{LO}}$ is at the order of several percent. We may contrast this with intrinsic limitations of absolute measurements at the LHC, like the determination of the overall scattering luminosity [104, 105] or our ability to resolve the energy of final-state radiation [106, 107], and compare this with the anticipated precision that will be reached by the LHC [108]. We conclude that phenomenological comparisons at the percent level for certain processes will be possible and that N³LO QCD corrections modify predictions at the same level of precision. Even higher precision will be achievable by considering ratios of processes that eliminate some of the shared uncertainties and developing predictions for targeted observables to extract physical information will play a crucial role.

Assessing the uncertainty of predictions due to the use of perturbative QFT is crucial. N³LO corrections for production processes represent the currently highest order achieved, and the size of these corrections can therefore inform us on the progression of corrections obtained with QFT perturbation theory. Regarding results for $\delta\sigma_X^{\text{NNLO}}$, we observe that much smaller corrections were obtained at N³LO than NNLO for gluon fusion Higgs production, and that the corrections are of comparable size for quark-initiated processes. Overall, our interpretation is that N³LO corrections lead to an improved description of scattering processes.

In previous sections, we studied the impact of perturbative scale variations on N³LO processes and the use of these scale variations as uncertainty estimates. We would like to re-emphasize here the importance of reliable uncertainty estimates and the exploration of alternative methods to set perturbative uncertainties beyond scale variations. Correlations of uncertainties between different bins of a distribution or between different perturbative observable of the same or different processes will have to be addressed in the future. First steps towards alternative methods beyond scale variation were investigated for example in refs. [26–28]. Nevertheless, using seven-point scale variations ($\delta(\text{scale})$) to estimate perturbative uncertainties, we observe in Table 5 that these are at the percent level for the processes we consider. This observation yet again emphasizes the importance for N³LO QCD computations to achieve percent-level precision in LHC phenomenology.

In the right-most two columns of Table 5 we collected uncertainties due to missing N³LO PDFs (see eq. (14)) and our imprecise knowledge of PDFs and the strong coupling constant (see eq. (13)). We observe that the associated uncertainties are of comparable size for all considered processes here and present currently some of the largest theoretical uncertainties on our predictions. We have studied in previous sections the impact of more modern PDF sets on cross section predictions and found a slight reduction of PDF uncertainties. Recently, new approximate N³LO PDFs were obtained in ref. [109], methods to quantify other theoretical uncertainties are discussed in ref. [110] and new methodologies to fit PDFs are explored for example in ref. [75]. We leave a more detailed study of these developments to future work but emphasize the importance of reliable PDF uncertainties due to their dominating role in theoretical predictions at N³LO.

6 Summary and conclusions

We performed a comprehensive phenomenological analysis of the fully-inclusive color-singlet production cross section at hadron colliders up to the third order in the strong coupling constant. Together with this article, we introduce the computer program `n3lox`, which allows us to numerically calculate inclusive N³LO cross sections for Higgs production in gluon fusion and $b\bar{b}$ annihilation and charged- and neutral-current Drell-Yan processes. In addition, our code allows us to integrate over the virtuality of the final state, which enables us to calculate associated Higgs boson production at N³LO using the known corrections for Drell-Yan processes.

We investigated scale uncertainties as a method of assessing theoretical uncertainties due to missing higher orders at different values of the center-of-mass energy and for pp and $p\bar{p}$ collisions. In most of the analyzed cases, the traditional 7-point scale variation at NNLO does not capture the N³LO central value. As a consequence, uncertainty estimates for missing higher orders based on scale variation alone should be taken with a grain of salt, already at NNLO. We note that Bayesian methods may offer in the future a viable alternative as they typically provide more significant uncertainties than the scale variation at NNLO, cf., e.g., refs. [26–28].

We compared the N³LO predictions for different PDF sets. We note significant overall progress in the past years in determining the PDF and their uncertainties. While minor observed discrepancies between various sets require dedicated studies within the PDF community, in the meantime a conservative approach would require taking the envelope of the predictions for all the modern sets to account for possible systematic bias. As the third-order QCD corrections become available and the LHC gathers more precise data, the missing N³LO PDF sets are emerging as the biggest obstacle for further improvement of precision phenomenology at the hadron colliders.

In addition to the Higgs and Drell-Yan cross sections, we presented for the first time associated VH production at N³LO. We find that the third-order correction amounts to about $\sim 1\%$ and is similar in size to the NNLO correction, similar to the case of Drell-Yan production. This is not surprising, given that the VH process involves the same partonic

coefficient functions as for the Drell-Yan process. We conclude that the inclusion of the third-order correction is vital for precise phenomenological predictions, and the current theoretical uncertainty is dominated by the parametric and PDF uncertainties, which are typically at the order of 2%.

Our results discussed in this article, together with the `n3loxs` code which is available as a repository at <https://github.com/jubaglio/n3loxs>, will help benchmark precision QCD calculations and phenomenological studies at the LHC.

Acknowledgments

RS is supported by the United States Department of Energy under Grant Contract DE-SC0012704. BM is supported by the United States Department of Energy, Contract DE-AC02-76SF00515.

A `n3loxs`

`n3loxs` is the cross section calculator developed for this paper. This appendix presents the code, how to install it, and how to use it. The default values of the physical parameters are presented in appendix B.

`n3loxs` is a public code written mainly in C++ and Python and allows the user to calculate up to N³LO in QCD the following observables:

1. Neutral Drell-Yan differential production cross section $Q^2 d\sigma/dQ^2$ as a function of the virtuality Q of the gauge boson, in the leptonic channel $pp(p\bar{p}) \rightarrow \gamma^*/Z^* \rightarrow \ell^+\ell^- + X$;
2. Charged-current Drell-Yan differential production cross section $Q^2 d\sigma/dQ^2$ as a function of the virtuality Q of the W boson, in the leptonic channel $pp(p\bar{p}) \rightarrow W^+ \rightarrow \ell^+\nu_\ell + X$ ($pp(p\bar{p}) \rightarrow W^- \rightarrow \ell^-\bar{\nu}_\ell + X$);
3. Higgs boson inclusive production cross section in the gluon fusion channel, $gg \rightarrow H + X$, both for pp and $p\bar{p}$ colliders;
4. Higgs boson inclusive production cross section in the bottom-quark fusion channel, in the five-flavor scheme, $b\bar{b} \rightarrow H + X$, both for pp and $p\bar{p}$ colliders;
5. Higgsstrahlung inclusive production cross section in the charged and neutral channels, $pp(p\bar{p}) \rightarrow W^\pm H + X$ and $pp(p\bar{p}) \rightarrow ZH + X$.

The user can also calculate binned cross sections for Drell-Yan processes in a given range for Q , that is the production cross section $\sigma(Q_{\min} \leq Q \leq Q_{\max})$, see appendix D.

A.1 Installation

The program is written in C++ and Python. It requires a C++11 compatible compiler, Python 3.5 or higher, as well as the LHAPDF library already installed on the user machine. GNU Scientific Library (gsl) version 2.6 or higher is also required and is shipped with the code for convenience.

First `gunzip` and `untar` the file `n3loxs.tar.gz` with `tar -xzf n3loxs.tar.gz`. This will unpack the program into the directory `./n3loxs`. Enter the main directory with `cd ./n3loxs`, containing the following source files and subdirectories,

- `gsl-2.6`: the subdirectory containing the source code for the gsl library;
- `include`: the subdirectory containing the C++ header files, in particular the various physical constants hardcoded in `./include/constants.h`;
- `LICENSE`: the GPL 3 license of the program;
- `Makefile`: the script used to compile the program;
- `makegsl.sh`: the script used to compile the gsl library;
- `n3loxs`: the Python main executable of the program;
- `n3loxs_parameters.in`: the default input file containing customizable physical parameters as well as various flags;
- `README.md`: the ReadMe file explaining how to compile and use the program;
- `src`: source code subdirectory containing sub-subdirectories according to the various processes implemented in the program as well as the source code for the strong coupling constant evolution.

The user shall start compiling the shipped gsl library with `./makegsl.sh`. Once gsl is compiled, make sure that the LHAPDF config program (`lhpdf-config`) is correctly assigned in the `./Makefile`. This is usually found by your computer when typing `lhpdf-config`, but in case the LHAPDF library has been installed in a custom directory, simply change the line

```
LHAPDFCONFIG = lhpdf-config
```

in the Makefile to

```
LHAPDFCONFIG = [absolute path to the LHAPDF installation]/bin/lhpdf-config
```

After this check all the subprograms needed by the main executable `n3loxs` can be compiled by typing `make all`. This will create two subdirectories, `./build` containing the `.o` files, and `./subprogs` containing the C++ subprograms for each process.

The main executable, `n3loxs`, accesses the C++ subprograms located in `./subprogs`. If the user changes the location of the main executable `n3loxs`, they have to update the 52nd line of the script so that it accesses correctly the subprograms. Instead of the line

```
maindir=maindirpid.stdout.strip('\n'),
```

it has to be replaced by the absolute path to the directory `n3loxs`

```
maindir='[absolute path of the directory n3loxs on the computer]'
```

A.2 Usage

The program accepts up to three arguments on the command line, as well as an optional flag:

- `-lattice lattice`: The lattice size is an integer used for the integration. If this argument is omitted the default value is `lattice=1000`.
- `-seed seed`: The seed is an integer that is used to initialize the pseudo-random-number generator. If the argument is omitted the default value is `seed=1`.
- `--filename filename`: The name of the input file if the user does not want to use the default file, `n3loxs_parameters.in`. Note that the user input file needs to have the same structure as the default input file, otherwise the program will not run correctly and produce ill-defined results.
- `--scale` or `--7point`: An optional flag to calculate in a single call to the program 16 different predictions for the renormalization scale being varied between 0.5 and 2 times the chosen central scales of the process, while the factorization scale is fixed by the user at a given value (`--scale` flag); or an optional flag to calculate the seven-point scale variation around the central scales of the process (`--7point` flag). The flags are mutually exclusive.

Note that the default lattice may be too coarse for high precision studies requiring a precision at the sub-percent level. This happens for example for scale variation studies. It is advised to use at least `lattice=10000` in such cases.

The user can modify a handful of parameters. The default values for the physical parameters are given in appendix B. The other parameters give the user control over the calculational framework:

- `process` Selector of the desired process to be calculated. Following options are available:

`process=1`: neutral Drell-Yan differential production cross section at a given Q value;

`process=2`: charged Drell-Yan W^+ differential production cross section at a given Q value;

`process=3`: charged Drell-Yan W^- differential production cross section at a given Q value;

- `process=4:` Higgsstrahlung W^+H inclusive production cross section, fixed scale;
- `process=5:` Higgsstrahlung W^-H inclusive production cross section, fixed scale;
- `process=6:` Higgsstrahlung ZH inclusive production cross section, fixed scale;
- `process=7:` Five-Flavor scheme $b\bar{b} \rightarrow H$ inclusive production cross section;
- `process=8:` Gluon fusion $gg \rightarrow H$ inclusive production cross section, either in the heavy-top limit (HTL) or in the Born-improved HTL;
- `process=9:` neutral Drell-Yan production cross section in the bin $Q_{\min} \leq Q \leq Q_{\max}$;
- `process=10:` charged Drell-Yan W^+ production cross section in the bin $Q_{\min} \leq Q \leq Q_{\max}$;
- `process=11:` charged Drell-Yan W^- production cross section in the bin $Q_{\min} \leq Q \leq Q_{\max}$;
- `process=12:` Higgsstrahlung W^+H inclusive production cross section, dynamical scale;
- `process=13:` Higgsstrahlung W^-H inclusive production cross section, dynamical scale;
- `process=14:` Higgsstrahlung ZH inclusive production cross section, dynamical scale.

- `order:` Perturbative order in QCD up to which the calculation will be performed. `order=0` for LO calculation, up to `order=3` for N³LO calculation. The default choice in the input file is `order=3`.
- `collider:` Choice of the collider type. `collider=0` for a pp collider (LHC), `collider=1` for a $p\bar{p}$ (Tevatron). The default choice in the input file is `collider=0`.
- `muf0:` User-defined central factorization scale μ_F^0 , in GeV. If `muf0=-1` (default choice in the input file), μ_F^0 is fixed internally to the default central scale of the process (see below).
- `xmuf:` Ratio of the factorization scale μ_F used in the calculation and the previously defined central factorization scale μ_F^0 , such that $x_{\mu_F} = \mu_F/\mu_F^0$. The default choice in the input file is `xmuf=1.0`, which corresponds to the factorization scale used in the calculation equal to the central scale $\mu_F = \mu_F^0$. This parameter is useful for calculating the factorization scale variation. Note that this is equivalent to a direct change of the central scale.

- **mur0**: User-defined central renormalization scale μ_R^0 , in GeV. If **mur0=-1** (default choice in the input file), μ_R^0 is fixed internally to the default central scale of the process (see below).
- **xmur**: Ratio of the renormalization scale μ_R used in the calculation and the previously defined central renormalization scale μ_R^0 , such that $x_{\mu_R} = \mu_R/\mu_R^0$. The default choice in the input file is **xmur=1.0**, which corresponds to the renormalization scale used in the calculation equal to the central scale $\mu_R = \mu_R^0$. This parameter is useful for calculating the renormalization scale variation. Note that this is equivalent to a direct change of the central scale. .

The default central scales are defined as follows:

- Neutral- and charged-current Drell-Yan processes: $\mu_F^0 = \mu_R^0 = Q$.
 - Charged Higgsstrahlung processes (fixed scale): $\mu_F^0 = \mu_R^0 = m_H + m_W$.
 - Charged Higgsstrahlung processes (dynamical scale): $\mu_F^0 = \mu_R^0 = M_{HW}$.
 - Neutral Higgsstrahlung process (fixed scale): $\mu_F^0 = \mu_R^0 = m_H + m_Z$.
 - Neutral Higgsstrahlung process (dynamical scale): $\mu_F^0 = \mu_R^0 = M_{HZ}$.
 - Bottom-quark fusion Higgs process: $\mu_F^0 = \frac{1}{4}(m_H + 2m_b)$, $\mu_R^0 = m_H$.
 - Gluon fusion Higgs process: $\mu_F^0 = \mu_R^0 = \frac{1}{2}m_H$.
- **mt_scheme**: Flag to control the framework of the gluon fusion process. If **mt_scheme=0**, the calculation is performed in the on-shell scheme for the top-quark mass, if **mt_scheme=1**, the $\overline{\text{MS}}$ scheme is used. The default choice in the input file is **mt_scheme=1**.
 - **htl_flag**: Flag to control the framework of the gluon fusion process. If **htl_flag=0**, the calculation is performed in the pure heavy-top limit (HTL). If **htl_flag=1**, the calculation is performed in the Born-improved HTL, where the results are rescaled by the full LO Born matrix elements. The default choice in the input file is **htl_flag=1**.
 - **ncdy_flag**: Flag to control the framework of the neutral Drell-Yan process. If **ncdy_flag=0**, only the off-shell photon contribution is taken into account. If **ncdy_flag=1**, all contributions are taken into account (Z , γ^* , the interference terms, as well as the non-decoupling top contributions due to the axial anomaly). The default choice in the input file is **ncdy_flag=1**.

B Parameters

Below we summarize all parameters used throughout the paper. These parameter values are used as default values in the `n3l0xs` program. The code uses some hardwired

parameters located in the file `include/constants.h`, whose modification requires re-compilation of the code. In particular, it uses $n_f = 5$ for the number of massless quarks used in the perturbative coefficients as well as in the β functions and anomalous dimensions. The Cabibbo–Kobayashi–Maskawa matrix elements are also stored in the same file and read

$$\begin{aligned}
|V_{ud}| &= 0.97446, & |V_{us}| &= 0.22452, & |V_{ub}| &= 0.00365, \\
|V_{cd}| &= 0.22438, & |V_{cs}| &= 0.97359, & |V_{cb}| &= 0.04214, \\
|V_{td}| &= 0.00896, & |V_{ts}| &= 0.04133, & |V_{tb}| &= 0.999105.
\end{aligned}
\tag{16}$$

In addition, there are other physical parameters that can be changed by the user in the file `n3loxs_parameters.in` which is the main input file of the code. Any parameter and flag in this file can be modified at will without recompiling the code. The default values of these parameters are as follow,

$$\begin{aligned}
v &= 246.221 \text{ GeV}, \\
m_W &= 80.398 \text{ GeV}, \\
m_Z &= 91.1876 \text{ GeV}, \\
m_H &= 125.09 \text{ GeV}, \\
m_t &= 172.5 \text{ GeV}, \\
m_b &= 4.58 \text{ GeV}, \\
\bar{m}_t(\bar{m}_t) &= 162.7 \text{ GeV}, \\
\bar{m}_b(\bar{m}_b) &= 4.18 \text{ GeV}, \\
\Gamma_W &= 2.085 \text{ GeV}, \\
\Gamma_Z &= 2.4952 \text{ GeV}, \\
\alpha_S(m_Z) &= 0.118, \\
1/\alpha(0) &= 137.035999084, \\
E_{\text{collider}} &= 13 \text{ TeV}, \\
Q &= 100 \text{ GeV}, \quad Q_{\text{min}} = 80 \text{ GeV}, \quad Q_{\text{max}} = 90 \text{ GeV}, \\
\text{PDF} &= \text{PDF4LHC15_nnlo_mc}, \quad \text{PDFset} = 0.
\end{aligned}
\tag{17}$$

Note that $\alpha_S(m_Z)$ is automatically chosen by the code in accordance with the PDF set selected by the user: This parameter cannot be changed independently and does not appear in the file `n3loxs_parameters.in`. For Drell-Yan processes, either Q or the set $Q_{\text{min}}/Q_{\text{max}}$ is used, but not both at the same time, depending on the process chosen.

Finally, let us note following relations:

$$\begin{aligned}
g_W &= \sqrt{\frac{8m_W^2 G_F}{\sqrt{2}}}, & m_Z &= \frac{m_W}{\cos \theta_W}, & G_F &= \frac{1}{\sqrt{2}v^2}, \\
e &= g_W \sin \theta_W, & \alpha &= \frac{m_W^2 \left(1 - \frac{m_W^2}{m_Z^2}\right)}{\pi v^2}.
\end{aligned}
\tag{18}$$

Note that the code uses either $1/\alpha(0)$ or the vacuum expectation value v , depending on the process chosen, but not both parameters at the same time.

C Inclusive cross sections for VH processes at various additional center-of-mass energies

We present in this appendix inclusive cross sections at N³LO in QCD for Higgsstrahlung production, $pp \rightarrow VH$, for c.m. energies $\sqrt{s} = 7, 8, 14$ TeV (LHC), 27 TeV (HE-HLC) and 100 TeV (FCC-hh). Results for the W^+H process can be found in Table 7, for the W^-H process in Table 8, and for the ZH process in Table 9.

\sqrt{s} [TeV]	$\sigma^{\text{N}^3\text{LO}}(W^+H)$ [pb]	$\delta(\text{scale})$ [%]	$\delta(\text{PDF})$ [%]	$\delta(\text{PDF} + \alpha_S)$ [%]	$\delta(\text{PDF-TH})$ [%]
7	0.390	$\begin{smallmatrix} +0.15 \\ -0.23 \end{smallmatrix}$	± 1.92	± 2.02	± 0.91
8	0.470	$\begin{smallmatrix} +0.18 \\ -0.25 \end{smallmatrix}$	± 1.86	± 1.98	± 1.05
14	0.969	$\begin{smallmatrix} +0.29 \\ -0.31 \end{smallmatrix}$	± 1.51	± 1.75	± 1.49
27	2.11	$\begin{smallmatrix} +0.38 \\ -0.37 \end{smallmatrix}$	± 1.45	± 1.79	± 1.70
100	8.56	$\begin{smallmatrix} +0.49 \\ -0.52 \end{smallmatrix}$	± 2.11	± 2.51	± 1.36

Table 7: Total cross section for associated Higgs production with a W^+ boson at N³LO in QCD, at a proton-proton collider at various c.m. energies \sqrt{s} in TeV for a dynamical central scale choice $\mu_0 = M_{HW}$. The PDF set PDF4LHC15_nnlo_mc has been used. The 7-point scale uncertainty as well as the symmetrical PDF, PDF+ α_S , and PDF-TH uncertainties (in percent) are also given.

\sqrt{s} [TeV]	$\sigma^{\text{N}^3\text{LO}}(W^-H)$ [pb]	$\delta(\text{scale})$ [%]	$\delta(\text{PDF})$ [%]	$\delta(\text{PDF} + \alpha_S)$ [%]	$\delta(\text{PDF-TH})$ [%]
7	0.218	$^{+0.22}_{-0.31}$	± 2.28	± 2.35	± 1.24
8	0.271	$^{+0.24}_{-0.32}$	± 2.14	± 2.23	± 1.34
14	0.620	$^{+0.32}_{-0.36}$	± 1.72	± 1.90	± 1.66
27	1.48	$^{+0.39}_{-0.43}$	± 1.57	± 1.85	± 1.82
100	6.79	$^{+0.46}_{-0.58}$	± 2.13	± 2.50	± 1.58

Table 8: The same as in Table 7, but for the W^-H process.

\sqrt{s} [TeV]	$\sigma^{\text{N}^3\text{LO}}(ZH)$ [pb]	$\delta(\text{scale})$ [%]	$\delta(\text{PDF})$ [%]	$\delta(\text{PDF} + \alpha_S)$ [%]	$\delta(\text{PDF-TH})$ [%]
7	0.322	$^{+0.15}_{-0.22}$	± 1.94	± 2.02	± 1.01
8	0.395	$^{+0.18}_{-0.24}$	± 1.88	± 1.98	± 1.15
14	0.869	$^{+0.28}_{-0.30}$	± 1.69	± 1.88	± 1.58
27	2.01	$^{+0.36}_{-0.36}$	± 1.56	± 1.87	± 1.80
100	8.93	$^{+0.43}_{-0.48}$	± 2.07	± 2.47	± 1.54

Table 9: The same as in Table 7, but for the ZH process and with $\mu_0 = M_{HZ}$.

\sqrt{s} [TeV]	$\sigma^{\text{N}^3\text{LO}}(W^+H)$ [pb]	$\delta(\text{scale})$ [%]	$\delta(\text{PDF})$ [%]	$\delta(\text{PDF} + \alpha_S)$ [%]	$\delta(\text{PDF-TH})$ [%]
7	0.390	$^{+0.19}_{-0.28}$	± 1.94	± 2.04	± 0.92
8	0.470	$^{+0.22}_{-0.30}$	± 1.87	± 1.99	± 1.06
14	0.968	$^{+0.30}_{-0.35}$	± 1.57	± 1.80	± 1.50
27	2.11	$^{+0.38}_{-0.41}$	± 1.47	± 1.81	± 1.71
100	8.56	$^{+0.46}_{-0.57}$	± 2.21	± 2.59	± 1.34

Table 10: The same as in Table 7, but with $\mu_0 = M_H + M_W$.

\sqrt{s} [TeV]	$\sigma^{\text{N}^3\text{LO}}(W^-H)$ [pb]	$\delta(\text{scale})$ [%]	$\delta(\text{PDF})$ [%]	$\delta(\text{PDF} + \alpha_S)$ [%]	$\delta(\text{PDF-TH})$ [%]
7	0.218	$^{+0.22}_{-0.31}$	± 2.28	± 2.35	± 1.25
8	0.271	$^{+0.24}_{-0.32}$	± 2.15	± 2.23	± 1.35
14	0.620	$^{+0.32}_{-0.36}$	± 1.74	± 1.92	± 1.67
27	1.48	$^{+0.39}_{-0.43}$	± 1.70	± 1.96	± 1.83
100	6.78	$^{+0.45}_{-0.58}$	± 2.18	± 2.54	± 1.57

Table 11: The same as in Table 8, but with $\mu_0 = M_H + M_W$.

\sqrt{s} [TeV]	$\sigma^{\text{N}^3\text{LO}}(ZH)$ [pb]	$\delta(\text{scale})$ [%]	$\delta(\text{PDF})$ [%]	$\delta(\text{PDF} + \alpha_S)$ [%]	$\delta(\text{PDF-TH})$ [%]
7	0.322	$\begin{smallmatrix} +0.18 \\ -0.27 \end{smallmatrix}$	± 1.98	± 2.06	± 1.02
8	0.395	$\begin{smallmatrix} +0.21 \\ -0.29 \end{smallmatrix}$	± 1.88	± 1.98	± 1.16
14	0.868	$\begin{smallmatrix} +0.29 \\ -0.33 \end{smallmatrix}$	± 1.71	± 1.90	± 1.58
27	2.01	$\begin{smallmatrix} +0.35 \\ -0.39 \end{smallmatrix}$	± 1.57	± 1.87	± 1.81
100	8.92	$\begin{smallmatrix} +0.40 \\ -0.52 \end{smallmatrix}$	± 2.11	± 2.50	± 1.52

Table 12: The same as in Table 9, but for $\mu_0 = M_H + M_Z$.

D Binned cross sections for Drell-Yan processes

n3l0xs can also calculate Drell-Yan cross sections in a given bin range of the invariant-mass distribution $Q_1 \leq Q \leq Q_2$:

$$\int_{Q_1^2}^{Q_2^2} dQ^2 \frac{d\sigma_{N_1 N_2 \rightarrow f_1 f_2 + X}}{dQ^2}. \quad (19)$$

Using eq. (19) we can produce the invariant-mass distribution in a binned form, in windows around the Z - or W -peak. As an example, we display in fig. 20 at the 13 TeV LHC for bin sizes of 5 GeV and 0.5 GeV respectively. By choosing the largest bin range possible, it is possible to obtain the total cross section for the processes $pp \rightarrow Z^*/\gamma^* \rightarrow \ell^+\ell^-$ and $pp \rightarrow W \rightarrow \ell\nu_\ell$ up to N³LO in QCD, using dynamical renormalization and factorization scales $\mu_R = \mu_F = Q$.

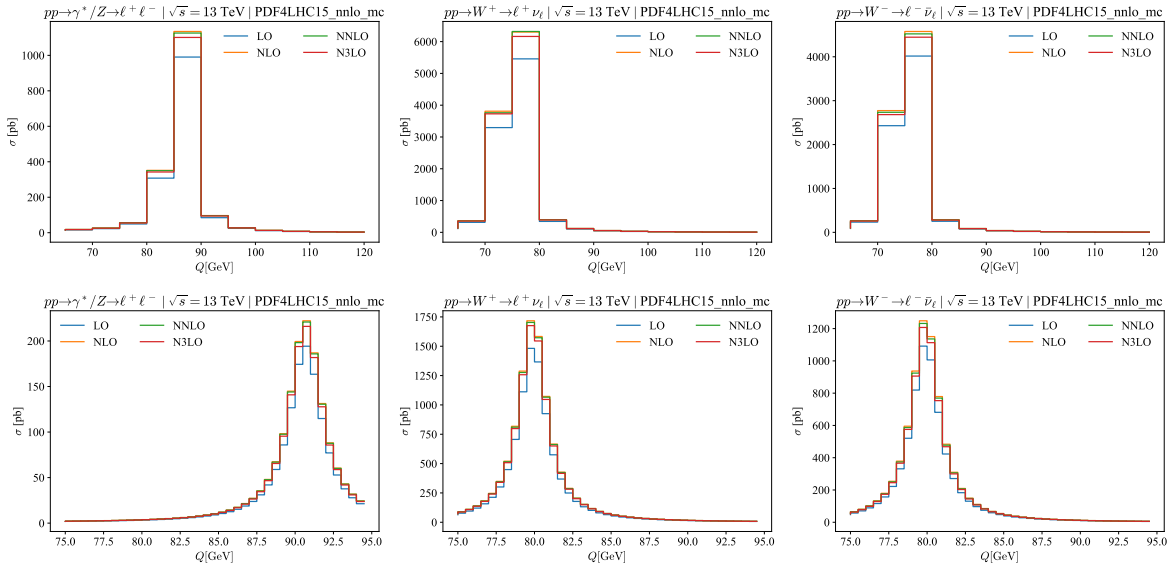


Figure 20: The invariant-mass distribution around the Z or W -peak for the neutral- and charged-current Drell-Yan processes at the 13 TeV LHC, in bins of size 5 GeV (upper panels) and 0.5 GeV (lower panels) respectively. Note that the y -axis on the upper panel is logarithmic.

References

- [1] C. Anastasiou, C. Duhr, F. Dulat, F. Herzog and B. Mistlberger, *Higgs Boson Gluon-Fusion Production in QCD at Three Loops*, *Phys. Rev. Lett.* **114** (2015) 212001 [[1503.06056](#)].

- [2] X. Chen, T. Gehrmann, E. W. N. Glover, A. Huss, B. Mistlberger and A. Pelloni, *Fully Differential Higgs Boson Production to Third Order in QCD*, *Phys. Rev. Lett.* **127** (2021) 072002 [[2102.07607](#)].
- [3] X. Chen, T. Gehrmann, N. Glover, A. Huss, T.-Z. Yang and H. X. Zhu, *Dilepton Rapidity Distribution in Drell-Yan Production to Third Order in QCD*, *Phys. Rev. Lett.* **128** (2022) 052001 [[2107.09085](#)].
- [4] S. Camarda, L. Cieri and G. Ferrera, *Drell-Yan lepton-pair production: qT resummation at N^3LL accuracy and fiducial cross sections at N^3LO* , *Phys. Rev. D* **104** (2021) L111503 [[2103.04974](#)].
- [5] T. Neumann and J. Campbell, *Fiducial Drell-Yan production at the LHC improved by transverse-momentum resummation at N^4LL+N^3LO* , [2207.07056](#).
- [6] X. Chen, T. Gehrmann, E. W. N. Glover, A. Huss, P. F. Monni, E. Re et al., *Third-Order Fiducial Predictions for Drell-Yan Production at the LHC*, *Phys. Rev. Lett.* **128** (2022) 252001 [[2203.01565](#)].
- [7] X. Chen, T. Gehrmann, N. Glover, A. Huss, T.-Z. Yang and H. X. Zhu, *Transverse Mass Distribution and Charge Asymmetry in W Boson Production to Third Order in QCD*, [2205.11426](#).
- [8] C. Anastasiou, C. Duhr, F. Dulat, E. Furlan, T. Gehrmann, F. Herzog et al., *Higgs boson gluon-fusion production at threshold in N^3LO QCD*, *Phys. Lett. B* **737** (2014) 325 [[1403.4616](#)].
- [9] C. Anastasiou, C. Duhr, F. Dulat, E. Furlan, T. Gehrmann, F. Herzog et al., *High precision determination of the gluon fusion Higgs boson cross-section at the LHC*, *JHEP* **05** (2016) 058 [[1602.00695](#)].
- [10] B. Mistlberger, *Higgs boson production at hadron colliders at N^3LO in QCD*, *JHEP* **05** (2018) 028 [[1802.00833](#)].
- [11] C. Anastasiou, C. Duhr, F. Dulat and B. Mistlberger, *Soft triple-real radiation for Higgs production at N^3LO* , *JHEP* **07** (2013) 003 [[1302.4379](#)].
- [12] C. Anastasiou, C. Duhr, F. Dulat, E. Furlan, F. Herzog and B. Mistlberger, *Soft expansion of double-real-virtual corrections to Higgs production at N^3LO* , *JHEP* **08** (2015) 051 [[1505.04110](#)].
- [13] C. Anastasiou, C. Duhr, F. Dulat, F. Herzog and B. Mistlberger, *Real-virtual contributions to the inclusive Higgs cross-section at N^3LO* , *JHEP* **12** (2013) 088 [[1311.1425](#)].
- [14] C. Anastasiou, C. Duhr, F. Dulat, E. Furlan, T. Gehrmann, F. Herzog et al., *Higgs Boson Gluon Fusion Production Beyond Threshold in N^3LO QCD*, *JHEP* **03** (2015) 091 [[1411.3584](#)].

- [15] F. A. Dreyer and A. Karlberg, *Vector-Boson Fusion Higgs Production at Three Loops in QCD*, *Phys. Rev. Lett.* **117** (2016) 072001 [[1606.00840](#)].
- [16] C. Duhr, F. Dulat and B. Mistlberger, *Drell-Yan Cross Section to Third Order in the Strong Coupling Constant*, *Phys. Rev. Lett.* **125** (2020) 172001 [[2001.07717](#)].
- [17] C. Duhr, F. Dulat and B. Mistlberger, *Charged current Drell-Yan production at N^3LO* , *JHEP* **11** (2020) 143 [[2007.13313](#)].
- [18] C. Duhr, F. Dulat and B. Mistlberger, *Higgs Boson Production in Bottom-Quark Fusion to Third Order in the Strong Coupling*, *Phys. Rev. Lett.* **125** (2020) 051804 [[1904.09990](#)].
- [19] C. Duhr, F. Dulat, V. Hirschi and B. Mistlberger, *Higgs production in bottom quark fusion: matching the 4- and 5-flavour schemes to third order in the strong coupling*, *JHEP* **08** (2020) 017 [[2004.04752](#)].
- [20] L.-B. Chen, H. T. Li, H.-S. Shao and J. Wang, *The gluon-fusion production of Higgs boson pair: N^3LO QCD corrections and top-quark mass effects*, *JHEP* **03** (2020) 072 [[1912.13001](#)].
- [21] F. A. Dreyer and A. Karlberg, *Vector-Boson Fusion Higgs Pair Production at N^3LO* , *Phys. Rev. D* **98** (2018) 114016 [[1811.07906](#)].
- [22] C. Duhr and B. Mistlberger, *Lepton-pair production at hadron colliders at N^3LO in QCD*, *JHEP* **03** (2022) 116 [[2111.10379](#)].
- [23] F. Dulat, A. Lazopoulos and B. Mistlberger, *$iHiggs$ 2 — Inclusive Higgs cross sections*, *Comput. Phys. Commun.* **233** (2018) 243 [[1802.00827](#)].
- [24] M. Bonvini, S. Marzani, C. Muselli and L. Rottoli, *On the Higgs cross section at N^3LO+N^3LL and its uncertainty*, *JHEP* **08** (2016) 105 [[1603.08000](#)].
- [25] R. V. Harlander, S. Liebler and H. Mantler, *SusHi Bento: Beyond NNLO and the heavy-top limit*, *Comput. Phys. Commun.* **212** (2017) 239 [[1605.03190](#)].
- [26] M. Cacciari and N. Houdeau, *Meaningful characterisation of perturbative theoretical uncertainties*, *JHEP* **09** (2011) 039 [[1105.5152](#)].
- [27] M. Bonvini, *Probabilistic definition of the perturbative theoretical uncertainty from missing higher orders*, *Eur. Phys. J. C* **80** (2020) 989 [[2006.16293](#)].
- [28] C. Duhr, A. Huss, A. Mazeliauskas and R. Szafron, *An analysis of Bayesian estimates for missing higher orders in perturbative calculations*, *JHEP* **09** (2021) 122 [[2106.04585](#)].
- [29] S. D. Drell and T.-M. Yan, *Massive Lepton Pair Production in Hadron-Hadron Collisions at High-Energies*, *Phys. Rev. Lett.* **25** (1970) 316.

- [30] G. Altarelli, R. K. Ellis and G. Martinelli, *Leptoproduction and Drell-Yan Processes Beyond the Leading Approximation in Chromodynamics*, *Nucl. Phys. B* **143** (1978) 521.
- [31] J. Kubar-Andre and F. E. Paige, *Gluon Corrections to the Drell-Yan Model*, *Phys. Rev. D* **19** (1979) 221.
- [32] G. Altarelli, R. K. Ellis and G. Martinelli, *Large Perturbative Corrections to the Drell-Yan Process in QCD*, *Nucl. Phys. B* **157** (1979) 461.
- [33] T. Matsuura and W. L. van Neerven, *Second Order Logarithmic Corrections to the Drell-Yan Cross-section*, *Z. Phys.* **C38** (1988) 623.
- [34] T. Matsuura, S. C. van der Marck and W. L. van Neerven, *The Order α_s^2 Contribution to the K Factor of the Drell-Yan Process*, *Phys. Lett.* **B211** (1988) 171.
- [35] T. Matsuura, S. C. van der Marck and W. L. van Neerven, *The Calculation of the Second Order Soft and Virtual Contributions to the Drell-Yan Cross-Section*, *Nucl. Phys.* **B319** (1989) 570.
- [36] R. Hamberg, W. L. van Neerven and T. Matsuura, *A complete calculation of the order α_s^2 correction to the Drell-Yan K factor*, *Nucl. Phys.* **B359** (1991) 343.
- [37] T. Matsuura, R. Hamberg and W. L. van Neerven, *The Contribution of the Gluon-gluon Subprocess to the Drell-Yan K Factor*, *Nucl. Phys.* **B345** (1990) 331.
- [38] W. L. van Neerven and E. B. Zijlstra, *The $O(\alpha_s^2)$ corrected Drell-Yan K factor in the DIS and \overline{MS} scheme*, *Nucl. Phys.* **B382** (1992) 11.
- [39] D. A. Dicus and S. Willenbrock, *Higgs Boson Production from Heavy Quark Fusion*, *Phys. Rev. D* **39** (1989) 751.
- [40] D. Dicus, T. Stelzer, Z. Sullivan and S. Willenbrock, *Higgs boson production in association with bottom quarks at next-to-leading order*, *Phys. Rev.* **D59** (1999) 094016 [[hep-ph/9811492](#)].
- [41] C. Balazs, H.-J. He and C. P. Yuan, *QCD corrections to scalar production via heavy quark fusion at hadron colliders*, *Phys. Rev.* **D60** (1999) 114001 [[hep-ph/9812263](#)].
- [42] J. M. Campbell, R. K. Ellis, F. Maltoni and S. Willenbrock, *Higgs-Boson Production in Association with a Single Bottom Quark*, *Phys. Rev. D* **67** (2003) 095002 [[hep-ph/0204093](#)].
- [43] F. Maltoni, Z. Sullivan and S. Willenbrock, *Higgs-Boson Production via Bottom-Quark Fusion*, *Phys. Rev. D* **67** (2003) 093005 [[hep-ph/0301033](#)].

- [44] R. V. Harlander and W. B. Kilgore, *Higgs boson production in bottom quark fusion at next-to-next-to leading order*, *Phys. Rev.* **D68** (2003) 013001 [[hep-ph/0304035](#)].
- [45] H. M. Georgi, S. L. Glashow, M. E. Machacek and D. V. Nanopoulos, *Higgs Bosons from Two Gluon Annihilation in Proton Proton Collisions*, *Phys. Rev. Lett.* **40** (1978) 692.
- [46] A. Djouadi, M. Spira and P. M. Zerwas, *Production of Higgs bosons in proton colliders: QCD corrections*, *Phys. Lett. B* **264** (1991) 440.
- [47] S. Dawson, *Radiative corrections to Higgs boson production*, *Nucl. Phys. B* **359** (1991) 283.
- [48] M. Spira, A. Djouadi, D. Graudenz and P. M. Zerwas, *Higgs boson production at the LHC*, *Nucl. Phys. B* **453** (1995) 17 [[hep-ph/9504378](#)].
- [49] R. V. Harlander and W. B. Kilgore, *Next-to-next-to-leading order Higgs production at hadron colliders*, *Phys. Rev. Lett.* **88** (2002) 201801 [[hep-ph/0201206](#)].
- [50] C. Anastasiou and K. Melnikov, *Higgs boson production at hadron colliders in NNLO QCD*, *Nucl. Phys. B* **646** (2002) 220 [[hep-ph/0207004](#)].
- [51] V. Ravindran, J. Smith and W. L. van Neerven, *NNLO corrections to the total cross-section for Higgs boson production in hadron hadron collisions*, *Nucl. Phys. B* **665** (2003) 325 [[hep-ph/0302135](#)].
- [52] R. V. Harlander and W. B. Kilgore, *Production of a pseudoscalar Higgs boson at hadron colliders at next-to-next-to leading order*, *JHEP* **10** (2002) 017 [[hep-ph/0208096](#)].
- [53] S. Marzani, R. D. Ball, V. Del Duca, S. Forte and A. Vicini, *Higgs production via gluon-gluon fusion with finite top mass beyond next-to-leading order*, *Nucl. Phys. B* **800** (2008) 127 [[0801.2544](#)].
- [54] A. Pak, M. Rogal and M. Steinhauser, *Finite top quark mass effects in NNLO Higgs boson production at LHC*, *JHEP* **02** (2010) 025 [[0911.4662](#)].
- [55] R. V. Harlander, H. Mantler, S. Marzani and K. J. Ozeren, *Higgs production in gluon fusion at next-to-next-to-leading order QCD for finite top mass*, *Eur. Phys. J. C* **66** (2010) 359 [[0912.2104](#)].
- [56] M. Czakon, R. V. Harlander, J. Klappert and M. Niggetiedt, *Exact Top-Quark Mass Dependence in Hadronic Higgs Production*, *Phys. Rev. Lett.* **127** (2021) 162002 [[2105.04436](#)].

- [57] F. Wilczek, *Decays of Heavy Vector Mesons into Higgs Particles*, *Physical Review Letters* **39** (1977) 1304.
- [58] V. P. Spiridonov and K. G. Chetyrkin, *Nonleading mass corrections and renormalization of the operators $m \bar{\psi} \psi$ and $g^{*2}(\mu \nu)$* , *Sov. J. Nucl. Phys.* **47** (1988) 522.
- [59] M. Shifman, A. Vainshtein and V. Zakharov, *Remarks on Higgs-boson interactions with nucleons*, *Physics Letters B* **78** (1978) 443.
- [60] T. Inami, T. Kubota and Y. Okada, *Effective Gauge Theory and the Effect of Heavy Quarks*, *Zeitschrift für Physik C* **18** (1983) 69.
- [61] Y. Schroder and M. Steinhauser, *Four-loop decoupling relations for the strong coupling*, *JHEP* **01** (2006) 051 [[hep-ph/0512058](#)].
- [62] M. Kramer, E. Laenen and M. Spira, *Soft gluon radiation in Higgs boson production at the LHC*, *Nucl. Phys.* **B511** (1998) 523 [[hep-ph/9611272](#)].
- [63] K. Chetyrkin, J. Kühn and C. Sturm, *QCD decoupling at four loops*, *Nuclear Physics B* **744** (2006) 121.
- [64] K. G. Chetyrkin, B. A. Kniehl and M. Steinhauser, *Decoupling relations to $\mathcal{O}(\alpha_s^3)$ and their connection to low-energy theorems*, *Nucl. Phys.* **B510** (1998) 61 [[hep-ph/9708255](#)].
- [65] W.-L. Ju and M. Schönherr, *The q_T and $\Delta\phi$ spectra in W and Z production at the LHC at $N^3LL'+N^2LO$* , *JHEP* **10** (2021) 088 [[2106.11260](#)].
- [66] L. Chen, M. Czakon and M. Niggetiedt, *The complete singlet contribution to the massless quark form factor at three loops in QCD*, *JHEP* **12** (2021) 095 [[2109.01917](#)].
- [67] J. Butterworth et al., *PDF4LHC recommendations for LHC Run II*, *J. Phys.* **G43** (2016) 023001 [[1510.03865](#)].
- [68] T. van Ritbergen, J. A. M. Vermaseren and S. A. Larin, *The Four loop beta function in quantum chromodynamics*, *Phys. Lett.* **B400** (1997) 379 [[hep-ph/9701390](#)].
- [69] M. Czakon, *The Four-loop QCD beta-function and anomalous dimensions*, *Nucl. Phys.* **B710** (2005) 485 [[hep-ph/0411261](#)].
- [70] P. A. Baikov, K. G. Chetyrkin and J. H. Kühn, *Five-Loop Running of the QCD coupling constant*, *Phys. Rev. Lett.* **118** (2017) 082002 [[1606.08659](#)].
- [71] F. Herzog, B. Ruijl, T. Ueda, J. A. M. Vermaseren and A. Vogt, *The five-loop beta function of Yang-Mills theory with fermions*, *JHEP* **02** (2017) 090 [[1701.01404](#)].

- [72] S. Bailey, T. Cridge, L. A. Harland-Lang, A. D. Martin and R. S. Thorne, *Parton distributions from LHC, HERA, Tevatron and fixed target data: MSHT20 PDFs*, *Eur. Phys. J. C* **81** (2021) 341 [[2012.04684](#)].
- [73] T.-J. Hou et al., *New CTEQ global analysis of quantum chromodynamics with high-precision data from the LHC*, *Phys. Rev. D* **103** (2021) 014013 [[1912.10053](#)].
- [74] NNPDF collaboration, R. D. Ball et al., *Parton distributions from high-precision collider data*, *Eur. Phys. J. C* **77** (2017) 663 [[1706.00428](#)].
- [75] NNPDF collaboration, R. D. Ball et al., *The path to proton structure at 1% accuracy*, *Eur. Phys. J. C* **82** (2022) 428 [[2109.02653](#)].
- [76] R. D. Ball et al., *The PDF4LHC21 combination of global PDF fits for the LHC Run III*, [2203.05506](#).
- [77] S. Alekhin, J. Blümlein, S. Moch and R. Placakyte, *Parton distribution functions, α_s , and heavy-quark masses for LHC Run II*, *Phys. Rev. D* **96** (2017) 014011 [[1701.05838](#)].
- [78] B. A. Kniehl, *Associated Production of Higgs and Z Bosons From Gluon Fusion in Hadron Collisions*, *Phys. Rev. D* **42** (1990) 2253.
- [79] L. Altenkamp, S. Dittmaier, R. V. Harlander, H. Rzehak and T. J. E. Zirke, *Gluon-induced Higgs-strahlung at next-to-leading order QCD*, *JHEP* **02** (2013) 078 [[1211.5015](#)].
- [80] J. Davies, G. Mishima and M. Steinhauser, *Virtual corrections to $gg \rightarrow ZH$ in the high-energy and large- m_t limits*, *JHEP* **03** (2021) 034 [[2011.12314](#)].
- [81] L. Chen, G. Heinrich, S. P. Jones, M. Kerner, J. Klappert and J. Schlenk, *ZH production in gluon fusion: two-loop amplitudes with full top quark mass dependence*, *JHEP* **03** (2021) 125 [[2011.12325](#)].
- [82] L. Alasfar, G. Degrossi, P. P. Giardino, R. Gröber and M. Vitti, *Virtual corrections to $gg \rightarrow ZH$ via a transverse momentum expansion*, *JHEP* **05** (2021) 168 [[2103.06225](#)].
- [83] G. Wang, X. Xu, Y. Xu and L. L. Yang, *Next-to-leading order corrections for $gg \rightarrow ZH$ with top quark mass dependence*, *Phys. Lett. B* **829** (2022) 137087 [[2107.08206](#)].
- [84] L. Chen, J. Davies, G. Heinrich, S. P. Jones, M. Kerner, G. Mishima et al., *ZH production in gluon fusion at NLO in QCD*, *JHEP* **08** (2022) 056 [[2204.05225](#)].
- [85] G. Degrossi, R. Gröber, M. Vitti and X. Zhao, *On the NLO QCD corrections to gluon-initiated ZH production*, *JHEP* **08** (2022) 009 [[2205.02769](#)].

- [86] O. Brein, R. Harlander, M. Wiesemann and T. Zirke, *Top-Quark Mediated Effects in Hadronic Higgs-Strahlung*, *Eur. Phys. J. C* **72** (2012) 1868 [[1111.0761](#)].
- [87] T. Han and S. Willenbrock, *QCD correction to the $pp \rightarrow WH$ and ZH total cross-sections*, *Phys. Lett. B* **273** (1991) 167.
- [88] H. Baer, B. Bailey and J. F. Owens, *$\mathcal{O}(\alpha_s)$ Monte Carlo approach to $W + Higgs$ associated production at hadron supercolliders*, *Phys. Rev. D* **47** (1993) 2730.
- [89] J. Ohnemus and W. J. Stirling, *Order α_s corrections to the differential cross-section for the WH intermediate mass Higgs signal*, *Phys. Rev. D* **47** (1993) 2722.
- [90] O. Brein, A. Djouadi and R. Harlander, *NNLO QCD corrections to the Higgs-strahlung processes at hadron colliders*, *Phys. Lett. B* **579** (2004) 149 [[hep-ph/0307206](#)].
- [91] O. Brein, R. V. Harlander and T. J. E. Zirke, *$vh@nnlo$ - Higgs Strahlung at hadron colliders*, *Comput. Phys. Commun.* **184** (2013) 998 [[1210.5347](#)].
- [92] R. V. Harlander, J. Klappert, S. Liebler and L. Simon, *$vh@nnlo-v2$: New physics in Higgs Strahlung*, *JHEP* **05** (2018) 089 [[1802.04817](#)].
- [93] G. Ferrera, M. Grazzini and F. Tramontano, *Associated WH production at hadron colliders: a fully exclusive QCD calculation at NNLO*, *Phys. Rev. Lett.* **107** (2011) 152003 [[1107.1164](#)].
- [94] G. Ferrera, M. Grazzini and F. Tramontano, *Associated ZH production at hadron colliders: the fully differential NNLO QCD calculation*, *Phys. Lett. B* **740** (2015) 51 [[1407.4747](#)].
- [95] G. Ferrera, M. Grazzini and F. Tramontano, *Higher-order QCD effects for associated WH production and decay at the LHC*, *JHEP* **04** (2014) 039 [[1312.1669](#)].
- [96] J. M. Campbell, R. K. Ellis and C. Williams, *Associated production of a Higgs boson at NNLO*, *JHEP* **06** (2016) 179 [[1601.00658](#)].
- [97] F. Caola, G. Luisoni, K. Melnikov and R. Röntsch, *NNLO QCD corrections to associated WH production and $H \rightarrow b\bar{b}$ decay*, *Phys. Rev. D* **97** (2018) 074022 [[1712.06954](#)].
- [98] G. Ferrera, G. Somogyi and F. Tramontano, *Associated production of a Higgs boson decaying into bottom quarks at the LHC in full NNLO QCD*, *Phys. Lett. B* **780** (2018) 346 [[1705.10304](#)].
- [99] I. Majer, *Associated Higgs Boson Production at NNLO QCD*, Ph.D. thesis, Zurich, ETH, Zurich, ETH, 2020. 10.3929/ethz-b-000448848.

- [100] R. Gauld, A. Gehrmann-De Ridder, E. W. N. Glover, A. Huss and I. Majer, *VH + jet production in hadron-hadron collisions up to order α_s^3 in perturbative QCD*, *JHEP* **03** (2022) 008 [[2110.12992](#)].
- [101] M. L. Ciccolini, S. Dittmaier and M. Kramer, *Electroweak radiative corrections to associated WH and ZH production at hadron colliders*, *Phys. Rev. D* **68** (2003) 073003 [[hep-ph/0306234](#)].
- [102] A. Denner, S. Dittmaier, S. Kallweit and A. Muck, *Electroweak corrections to Higgs-strahlung off W/Z bosons at the Tevatron and the LHC with HAWK*, *JHEP* **03** (2012) 075 [[1112.5142](#)].
- [103] F. Caola, W. Chen, C. Duhr, X. Liu, B. Mistlberger, F. Petriello et al., *The Path forward to N^3 LO*, in *2022 Snowmass Summer Study*, 3, 2022, [2203.06730](#).
- [104] ATLAS collaboration, *Luminosity determination in pp collisions at $\sqrt{s} = 13$ TeV using the ATLAS detector at the LHC*, .
- [105] CMS collaboration, A. M. Sirunyan et al., *Precision luminosity measurement in proton-proton collisions at $\sqrt{s} = 13$ TeV in 2015 and 2016 at CMS*, *Eur. Phys. J. C* **81** (2021) 800 [[2104.01927](#)].
- [106] CMS collaboration, V. Khachatryan et al., *Jet energy scale and resolution in the CMS experiment in pp collisions at 8 TeV*, *JINST* **12** (2017) P02014 [[1607.03663](#)].
- [107] ATLAS collaboration, M. Aaboud et al., *Jet energy scale measurements and their systematic uncertainties in proton-proton collisions at $\sqrt{s} = 13$ TeV with the ATLAS detector*, *Phys. Rev. D* **96** (2017) 072002 [[1703.09665](#)].
- [108] A. Dainese, M. Mangano, A. B. Meyer, A. Nisati, G. Salam and M. A. Vesterinen, eds., *Report on the Physics at the HL-LHC, and Perspectives for the HE-LHC*, vol. 7/2019 of *CERN Yellow Reports: Monographs*. CERN, Geneva, Switzerland, 2019, [10.23731/CYRM-2019-007](#).
- [109] J. McGowan, T. Cridge, L. A. Harland-Lang and R. S. Thorne, *Approximate N^3 LO Parton Distribution Functions with Theoretical Uncertainties: MSHT20a N^3 LO PDFs*, [2207.04739](#).
- [110] Z. Kassabov, M. Ubiali and C. Voisey, *Parton distributions with scale uncertainties: a MonteCarlo sampling approach*, [2207.07616](#).